GEOTECHNICAL EARTHQUAKE ENGINEERING

STEVEN L. KRAMER

11

Seismic Design of Retaining Walls

11.1 INTRODUCTION

Earth retaining structures, such as retaining walls, bridge abutments, quay walls, anchored bulkheads, braced excavations, and mechanically stabilized walls, are used throughout seismically active areas. They frequently represent key elements of ports and harbors, transportation systems, lifelines, and other constructed facilities. Earthquakes have caused permanent deformation of retaining structures in many historical earthquakes. In some cases, these deformations were negligibly small; in others they caused significant damage. In some cases, retaining structures have collapsed during earthquakes, with disastrous physical and economic consequences. This chapter discusses the behavior of retaining walls during earthquakes and presents several of the most common approaches to the seismic design of different types of retaining walls.

11.2 TYPES OF RETAINING WALLS

The problem of retaining soil is one of the oldest in geotechnical engineering; some of the earliest and most fundamental principles of soil mechanics were developed to allow rational design of retaining walls. Many different approaches to soil retention have been developed and used successfully. In recent years, the development of metallic, polymer, and geotextile reinforcement has led to the development of many innovative types of mechanically stabilized earth retention systems.

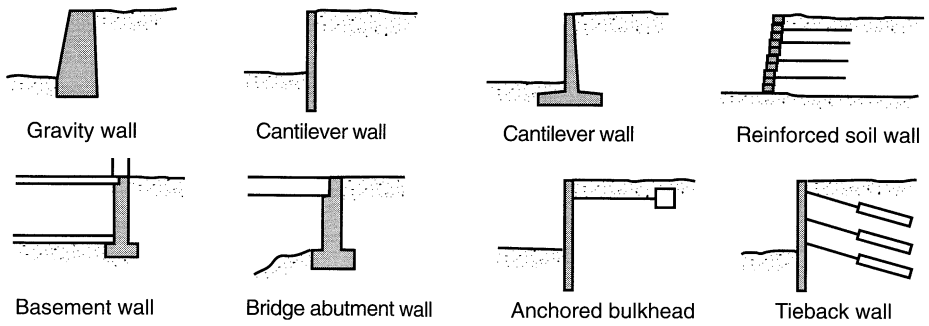

Figure 11.1 Common types of earth retaining structures.

Retaining walls are often classified in terms of their relative mass, flexibility, and anchorage conditions. *Gravity walls* (Figure 11.1) are the oldest and simplest type of retaining wall. Gravity walls are thick and stiff enough that they do not bend; their movement occurs essentially by rigid-body translation and/or rotation. Certain types of composite wall systems, such as crib walls and mechanically stabilized walls, are thick enough that they bend very little and consequently are often designed as gravity walls (with appropriate consideration of internal stability). *Cantilever walls*, which bend as well as translate and rotate, rely on their flexural strength to resist lateral earth pressures. The actual distribution of lateral earth pressure on a cantilever wall is influenced by the relative stiffness and deformation of both the wall and the soil. *Braced walls* are constrained against certain types of movement by the presence of external bracing elements. In the cases of basement walls and bridge abutment walls, lateral movements of the tops of the walls may be restrained by the structures they support. Tieback walls and anchored bulkheads are restrained against lateral movement by anchors embedded in the soil behind the walls. The provision of lateral support at different locations along a braced wall may keep bending moments so low that relatively flexible structural sections can be used.

11.3 TYPES OF RETAINING WALL FAILURES

To design retaining walls, it is necessary to define "failure" and to know how walls can fail. Under static conditions, retaining walls are acted upon by body forces related to the mass of the wall, by soil pressures, and by external forces such as those transmitted by braces. A properly designed retaining wall will achieve equilibrium of these forces without inducing shear stresses that approach the shear strength of the soil. During an earthquake, however, inertial forces and changes in soil strength may violate equilibrium and cause permanent deformation of the wall. Failure, whether by sliding, tilting, bending, or some other mechanism, occurs when these permanent deformations become excessive. The question of what level of deformation is excessive depends on many factors and is best addressed on a site-specific basis.

Gravity walls usually fail by rigid-body mechanisms such as sliding and/or overturning or by gross instability (Figure 11.2). Sliding occurs when horizontal force equilibrium is not maintained (i.e., when the lateral pressures on the back of the wall produce a thrust

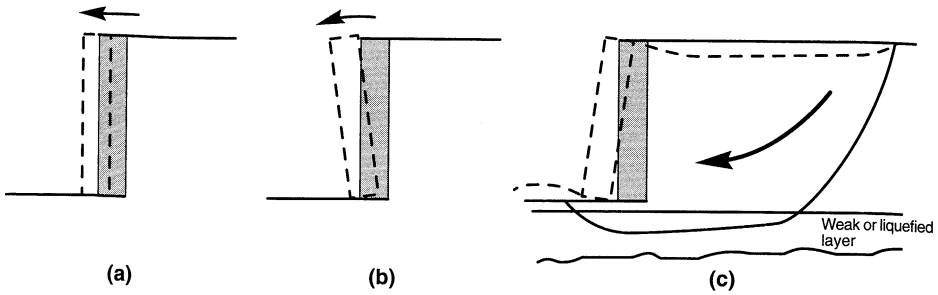

Figure 11.2 Typical failure mechanisms for a gravity retaining wall: (a) sliding (translational) failure; (b) overturning (rotational) failure; (c) gross instability failure.

that exceeds the available sliding resistance on the base of the wall). Overturning failures occur when moment equilibrium is not satisfied; bearing failures at the base of the wall are often involved. Gravity walls may also be damaged by gross instability of the soils behind and beneath them. Such failures may be treated as slope stability failures that encompass the wall. Composite wall systems, such as crib walls, bin walls, and mechanically stabilized walls, can fail in the same ways or by a number of internal mechanisms that may involve shearing, pullout, or tensile failure of various wall elements.

Cantilever walls are subject to the same failure mechanisms as gravity walls, and also to flexural failure mechanisms. Soil pressures and bending moments in cantilever walls depend on the geometry, stiffness, and strength of the wall–soil system (Figure 11.3a,b; pressure and moment diagrams for typical wall). If the bending moments required for equilibrium exceed the flexural strength of the wall, flexural failure may occur (Figure 11.3c). The structural ductility of the wall itself may influence the level of deformation produced by flexural failure.

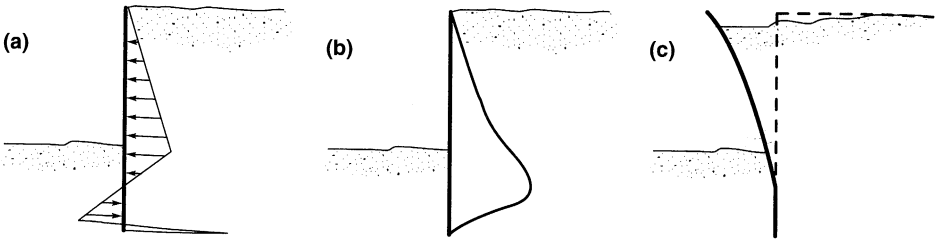

Figure 11.3 (a) Soil pressures, (b) bending moments, and (c) flexural failure mechanism for cantilever retaining wall.

Braced walls usually fail by gross instability, tilting, flexural failure, and/or failure of bracing elements. Tilting of braced walls typically involves rotation about the point at which the brace acts on the wall, often the top of the wall as in the cases of basement and bridge abutment walls (Figure 11.4a). Anchored walls with inadequate penetration may tilt by "kicking out" at their toes (Figure 11.4b). As in the case of cantilever walls, anchored walls may fail in flexure, although the point of failure (maximum bending moment) is likely to be different. Failure of bracing elements can include anchor pullout, tierod failure, or

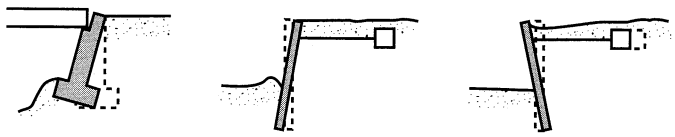

Figure 11.4 Potential modes of failure for braced walls: (a) rotation of bridge abutment about top; (b) rotation of anchored bulkhead due to lack of passive resistance ("kick-out") at the toe; (c) lack of adequate anchor capacity.

bridge buckling. Backfill settlements can also impose additional axial and transverse loading on bracing elements such as tierods and tiebacks.

11.4 STATIC PRESSURES ON RETAINING WALLS

The seismic behavior of retaining walls depends on the total lateral earth pressures that develop during earthquake shaking. These total pressures include both the static gravitational pressures that exist before an earthquake occurs, and the transient dynamic pressures induced by the earthquake. Since the response of a wall is influenced by both, a brief review of static earth pressures is presented.

Static earth pressures on retaining structures are strongly influenced by wall and soil movements. *Active earth pressures* develop as a retaining wall moves away from the soil behind it, inducing extensional lateral strain in the soil. When the wall movement is sufficient to fully mobilize the strength of the soil behind the wall, *minimum active earth pressures* act on the wall. Because very little wall movement is required to develop minimum active earth pressures (for the usual case of cohesionless backfill materials), free-standing retaining walls are usually designed on the basis of minimum active earth pressures. Where lateral wall movements are restrained, such as in the cases of tieback walls, anchored bulkheads, basement walls, and bridge abutments, static earth pressures may be greater than minimum active. *Passive earth pressures* develop as a retaining wall moves toward the soil, thereby producing compressive lateral strain in the soil. When the strength of the soil is fully mobilized, *maximum passive earth pressures* act on the wall. The stability of many free-standing retaining walls depends on the balance between active pressures acting predominantly on one side of the wall and passive pressures acting on the other.

Even under static conditions, prediction of actual retaining walls forces and deformations is a complicated soil–structure interaction problem. Deformations are rarely considered explicitly in design—the typical approach is to estimate the forces acting on a wall and then to design the wall to resist those forces with a factor of safety high enough to produce acceptably small deformations. A number of simplified approaches are available to evaluate static loads on retaining walls. The most commonly used are described in the following sections.

11.4.1 Rankine Theory

Rankine (1857) developed the simplest procedure for computing minimum active and maximum passive earth pressures. By making assumptions about the stress conditions and

strength envelope of the soil behind a retaining wall (the *backfill soil*), Rankine was able to render the lateral earth pressure problem determinate and directly compute the static pressures acting on retaining walls.

For minimum active conditions, Rankine expressed the pressure at a point on the back of a retaining wall as

$$p_A = K_A \sigma'_v - 2c\sqrt{K_A} \tag{11.1}$$

where K_A is the *coefficient of minimum active earth pressure*, σ'_v is the vertical effective stress at the point of interest, and c is the cohesive strength of the soil. When the principal stress planes are vertical and horizontal (as in the case of a smooth vertical wall retaining a horizontal backfill), the coefficient of minimum active earth pressure is given by

$$K_A = \frac{1 - \sin\phi}{1 + \sin\phi} = \tan^2\left(45 - \frac{\phi}{2}\right) \tag{11.2}$$

For the case of a cohesionless backfill inclined at an angle β with the horizontal, infinite slope solutions can be used (Terzaghi, 1943; Taylor, 1948) to compute K_A as

$$K_A = \cos\beta \frac{\cos\beta - \sqrt{\cos^2\beta - \cos^2\phi}}{\cos\beta + \sqrt{\cos^2\beta - \cos^2\phi}} \tag{11.3}$$

for $\beta \leq \phi$ [equation (11.3) is equivalent to equation (11.2) when $\beta = 0$]. The pressure distribution on the back of the wall, as indicated by equations (11.1), depends on the relative magnitudes of the frictional and cohesive components of the backfill soil strength (Figure 11.5). Although the presence of cohesion indicates that tensile stresses will develop between the upper portion of the wall and the backfill, tensile stresses do not actually develop in the field. The creep, stress relaxation, and low-permeability characteristics of cohesive soils render them undesirable as backfill material for retaining structures, and their use in that capacity is generally avoided whenever possible. For dry homogeneous cohesionless backfill, Rankine theory predicts a triangular active pressure distribution oriented parallel to the backfill surface. The active earth pressure resultant, P_A, acts at a point located $H/3$ above the base of a wall of height, H (Figure 11.5a) with magnitude

$$P_A = \tfrac{1}{2} K_A \gamma H^2 \tag{11.4}$$

Under maximum passive conditions, Rankine theory predicts wall pressures given by

$$p_P = K_p \sigma'_v + 2c\sqrt{K_p} \tag{11.5}$$

where K_P is the *coefficient of maximum passive earth pressure*. For smooth, vertical walls retaining horizontal backfills,

$$K_P = \frac{1 + \sin\phi}{1 - \sin\phi} = \tan^2\left(45 + \frac{\phi}{2}\right) \tag{11.6}$$

and

$$K_P = \cos\beta \frac{\cos\beta + \sqrt{\cos^2\beta - \cos^2\phi}}{\cos\beta - \sqrt{\cos^2\beta - \cos^2\phi}} \tag{11.7}$$

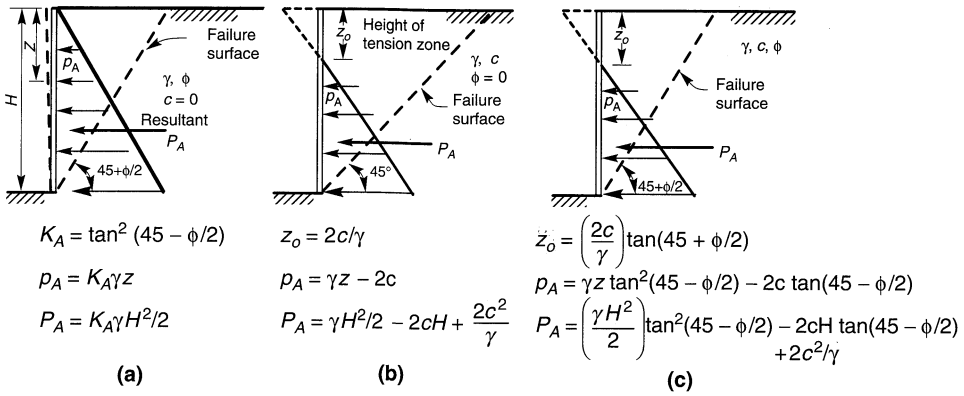

Figure 11.5 Minimum Rankine active earth pressure distributions for backfills with various combinations of frictional and cohesive strength: (a) frictional resistance, no cohesion; (b) cohesive soil, no frictional resistance; (c) combined cohesion and friction. (After NAVFAC, 1982.)

for backfills inclined at β to the horizontal. Passive pressure distributions for various backfill strength characteristics are shown in Figure 11.6. For a dry homogeneous backfill, Rankine theory predicts a triangular passive pressure distribution oriented parallel to the backfill surface. The passive earth pressure resultant, or *passive thrust*, P_P, acts at a point located $H/3$ above the base of a wall of height H (Figure 11.6a) with magnitude

$$P_P = \tfrac{1}{2} K_P \gamma H^2 \tag{11.8}$$

The presence of water in the backfill behind a retaining wall influences the effective stresses and hence the lateral earth pressure that acts on the wall. For wall design the hydrostatic

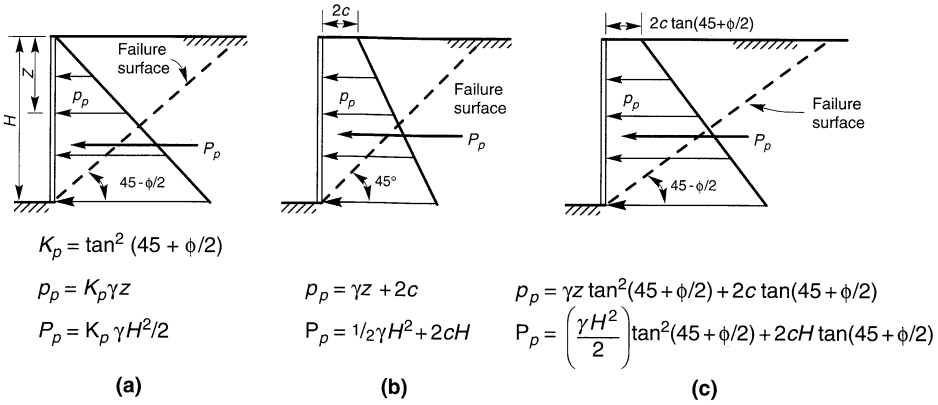

Figure 11.6 Maximum Rankine passive earth pressure distributions for backfills with various combinations of frictional and cohesive strength: (a) frictional resistance, no cohesion; (b) cohesive soil, no frictional resistance; (c) combined cohesion and friction. (After NAVFAC, 1982.)

pressure due to the water must be added to the lateral earth pressure. Because the total lateral thrust on a wall retaining a saturated backfill is considerably greater than that on a wall retaining dry backfill, the provision of backfill drainage is an important part of retaining wall design.

11.4.2 Coulomb Theory

Coulomb (1776) was the first to study the problem of lateral earth pressures on retaining structures. By assuming that the force acting on the back of a retaining wall resulted from the weight of a wedge of soil above a planar failure surface, Coulomb used force equilibrium to determine the magnitude of the soil thrust acting on the wall for both minimum active and maximum passive conditions. Since the problem is indeterminate, a number of potential failure surfaces must be analyzed to identify the critical failure surface (i.e., the surface that produces the greatest active thrust or the smallest passive thrust).

Under minimum active earth pressure conditions, the active thrust on a wall with the geometry shown in Figure 11.7a is obtained from force equilibrium (Figure 11.7b). For the critical failure surface, the active thrust on a wall retaining a cohesionless soil can be expressed as

$$P_A = \tfrac{1}{2} K_A \gamma H^2 \tag{11.9}$$

where

$$K_A = \frac{\cos^2(\phi - \theta)}{\cos^2\theta \cos(\delta + \theta)\left[1 + \sqrt{\dfrac{\sin(\delta + \phi)\sin(\phi - \beta)}{\cos(\delta + \theta)\cos(\beta - \theta)}}\right]^2} \tag{11.10}$$

δ is the angle of interface friction between the wall and the soil (Table 11-1), and β and θ are as shown in Figure 11.7a. The critical failure surface is inclined at an angle

$$\alpha_A = \phi + \tan^{-1}\left[\frac{\tan(\phi - \beta) + C_1}{C_2}\right] \tag{11.11}$$

to the horizontal where

$$C_1 = \sqrt{\tan(\phi - \beta)\,[\tan(\phi - \beta) + \cot(\phi - \theta)]\,[1 + \tan(\delta + \theta)\cot(\phi - \theta)]}$$

$$C_2 = 1 + \{\tan(\delta + \theta)\,[\tan(\phi - \beta) + \cot(\phi - \theta)]\}$$

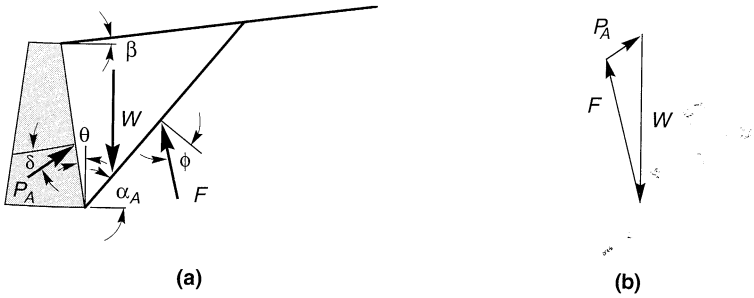

Figure 11.7 (a) Triangular active wedge bounded by planar backfill surface, failure surface, and wall; (b) force polygon for active Coulomb wedge. The critical failure surface is that which gives the largest value of P_A.

Table 11-1 Typical Interface Friction Angles

	Interface Materials	Interface Friction Angle δ
Mass concrete against:	clean sound rock	25
	clean gravel, gravel–sand mixtures, coarse sand	29–31
	clean fine to medium sand, silty medium to coarse sand, silty or clayey gravel	24–29
	clean fine sand, silty or clayey fine to medium sand	19–24
	fine sandy silt, nonplastic silt	17–19
Formed concrete against:	medium-stiff and stiff clay and silty clay	17–19
	clean gravel, gravel–sand mixture, well-graded rock fill with spalls	22–26
	clean sand, silty sand–gravel mixture, single-size hard rock fill	17–22
Steel sheet piles against:	silty sand, gravel, or sand mixed with silt or clay	17
	fine sandy silt, nonplastic silt	
	clean gravel, gravel–sand mixture, well-graded rock fill with spalls	14
		22
	clean sand, silty sand–gravel mixture, single-size hard rock fill	17
		14
	silty sand, gravel, or sand mixed with silt or clay	11
	fine sandy silt, nonplastic silt	

Source: After NAVFAC (1982).

Coulomb theory does not explicitly predict the distribution of active pressure, but it can be shown to be triangular for linear backfill surfaces with no surface loads. In such cases, P_A acts at a point located $H/3$ above the height of a wall of height H.

For maximum passive conditions in cohesionless backfills (Figure 11.8), Coulomb theory predicts a passive thrust

$$P_P = \tfrac{1}{2}K_P\gamma H^2 \tag{11.12}$$

where

$$K_P = \frac{\cos^2(\phi + \theta)}{\cos^2\theta\cos(\delta - \theta)\left[1 + \sqrt{\dfrac{\sin(\delta + \phi)\sin(\phi + \beta)}{\cos(\delta - \theta)\cos(\beta - \theta)}}\right]^2} \tag{11.13}$$

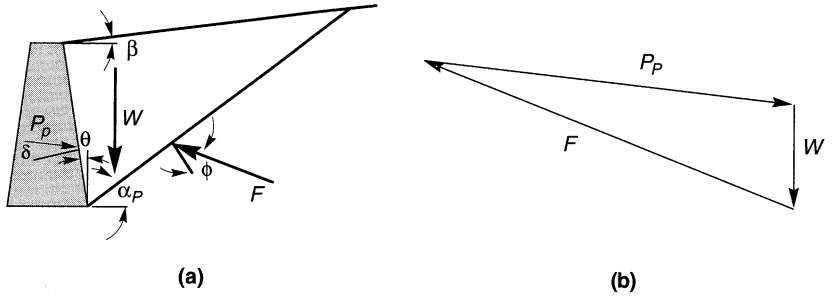

Figure 11.8 (a) Triangular passive wedge bounded by planar backfill surface, failure surface, and wall; (b) force polygon for passive Coulomb wedge. The critical failure surface is that which gives the largest value of P_P.

The critical failure surface for maximum passive earth pressure conditions is inclined to the horizontal at

$$\alpha_P = -\phi + \tan^{-1}\left[\frac{\tan(\phi+\beta)+C_3}{C_4}\right] \tag{11.14}$$

where

$$C_3 = \sqrt{\tan(\phi+\beta)\,[\tan(\phi+\beta)+\cot(\phi+\theta)]\,[1+\tan(\delta-\theta)\cot(\phi+\theta)]}$$

$$C_4 = 1+\{\tan(\delta-\theta)\,[\tan(\phi+\beta)+\cot(\phi+\theta)]\}$$

In contrast to Rankine theory, Coulomb theory can be used to predict soil thrusts on walls with irregular backfill slopes, concentrated loads on the backfill surface, and seepage forces. By considering the soil above a potential failure plane as a free body and including forces due to concentrated loads, boundary water pressures, and so on, the magnitude of the resultant thrust (P_A or P_P) can easily be computed.

11.4.3 Logarithmic Spiral Method

Although the major principal stress axis may be nearly perpendicular to the backfill surface at some distance behind a rough ($\delta > 0$) wall, the presence of shear stresses on the wall–soil interface can shift its position near the back of the wall. If the inclination of the principal stress axes varies within the backfill, the inclination of the failure surface must also vary. In other words, the failure surface must be curved. A logarithmic spiral function has been used to describe such curved failure surfaces for active and passive earth pressure conditions.

For active earth pressure conditions, the critical failure surface consists of a curved portion near the back of the wall and a linear portion that extends up to the ground surface (Figure 11.9a). The active earth pressure distribution is triangular (Figure 11.9b) for walls retaining planar, cohesionless backfills. Thus the active soil thrust can be expressed in the same form as equation (11.4), where the log spiral coefficients of minimum active earth pressure for various wall and backfill inclinations are given in Table 11-2. The active earth pressure coefficients given by the log spiral approach are generally considered to be slightly more accurate than those given by Rankine or Coulomb theory, but the difference is so small that the more convenient Coulomb approach is usually used.

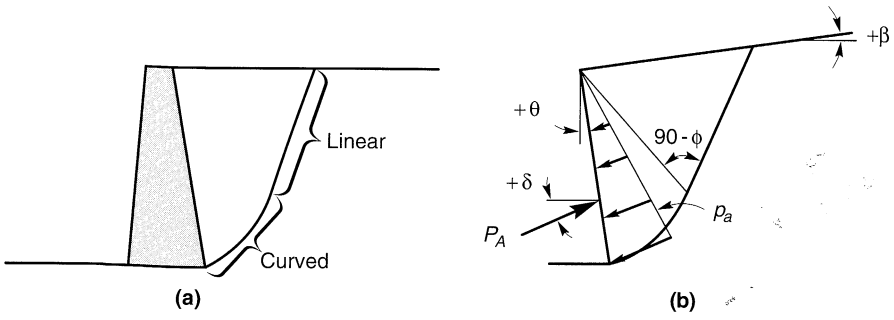

Figure 11.9 (a) Logarithmic spiral representation of the critical failure surface for minimum active earth pressure conditions; (b) orientation of critical failure surface for nonvertical wall with inclined backfill surface.

Table 11-2 Values for K_A for Log-Spiral Failure Surface

			ϕ					
δ	β	θ	20°	25°	30°	35°	40°	45°
0°	−15°	−10°	0.37	0.30	0.24	0.19	0.14	0.11
		0°	0.42	0.35	0.29	0.24	0.19	0.16
		10°	0.45	0.39	0.34	0.29	0.24	0.21
0°	0°	−10°	0.42	0.34	0.27	0.21	0.16	0.12
		0°	0.49	0.41	0.33	0.27	0.22	0.17
		10°	0.55	0.47	0.40	0.34	0.28	0.24
0°	15°	−10°	0.55	0.41	0.32	0.23	0.17	0.13
		0°	0.65	0.51	0.41	0.32	0.25	0.20
		10°	0.75	0.60	0.49	0.41	0.34	0.28
ϕ	−15°	−10°	0.31	0.26	0.21	0.17	0.14	0.11
		0°	0.37	0.31	0.26	0.23	0.19	0.17
		10°	0.41	0.36	0.31	0.27	0.25	0.23
ϕ	0°	−10°	0.37	0.30	0.24	0.19	0.15	0.12
		0°	0.44	0.37	0.30	0.26	0.22	0.19
		10°	0.50	0.43	0.38	0.33	0.30	0.26
ϕ	15°	−10°	0.50	0.37	0.29	0.22	0.17	0.14
		0°	0.61	0.48	0.37	0.32	0.25	0.21
		10°	0.72	0.58	0.46	0.42	0.35	0.31

Source: After Caquot and Kerisel (1948).

The effect of wall friction on the shape of the critical failure surface is more noticeable for passive earth pressure conditions. The passive failure surface also has curved and linear portions (Figure 11.10a), but the curved portion is much more pronounced than for active conditions. For planar cohesionless backfills, the passive earth pressure distribution is triangular (Figure 11.10b), so the passive thrust can be expressed in the form of equation (11.8), where the log spiral coefficients of maximum passive earth pressure are as given in Table 11-3. The passive earth pressure coefficients given by the log spiral method are

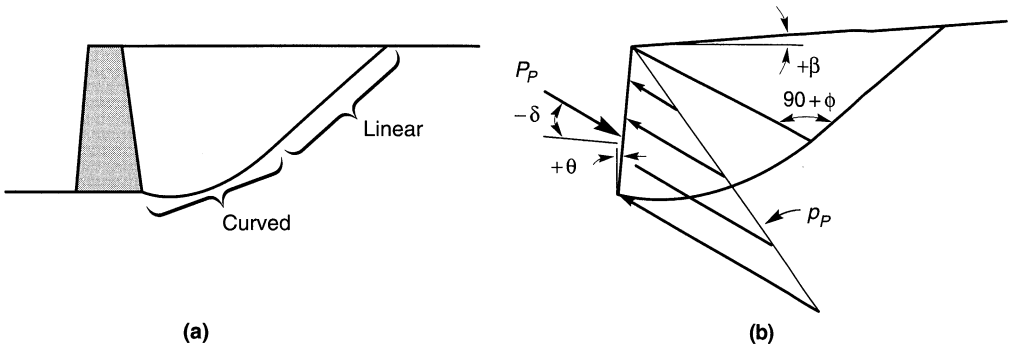

Figure 11.10 (a) Logarithmic spiral representation of the critical failure surface for maximum passive earth pressure conditions; (b) orientation of critical failure surface for nonvertical wall with inclined backfill surface.

Table 11-3 Values for K_P for Log-Spiral Failure Surface

			ϕ					
δ	β	θ	20°	25°	30°	35°	40°	45°
0°	−15°	−10°	1.32	1.66	2.05	2.52	3.09	3.95
		0°	1.09	1.33	1.56	1.82	2.09	2.48
		10°	0.87	1.03	1.17	1.30	1.33	1.54
0°	0°	−10°	2.33	2.96	3.82	5.00	6.68	9.20
		0°	2.04	2.46	3.00	3.69	4.59	5.83
		10°	1.74	1.89	2.33	2.70	3.14	3.69
0°	15°	−10°	3.36	4.56	6.30	8.98	12.2	20.0
		0°	2.99	3.86	5.04	6.72	10.4	12.8
		10°	2.63	3.23	3.97	4.98	6.37	8.20
ϕ	−15°	−10°	1.95	2.90	4.39	6.97	11.8	22.7
		0°	1.62	2.31	3.35	5.04	7.99	14.3
		10°	1.29	1.79	2.50	3.58	5.09	8.86
ϕ	0°	−10°	3.45	5.17	8.17	13.8	25.5	52.9
		0°	3.01	4.29	6.42	10.2	17.5	33.5
		10°	2.57	3.50	4.98	7.47	12.0	21.2
ϕ	15°	−10°	4.95	7.95	13.5	24.8	50.4	115
		0°	4.42	6.72	10.8	18.6	39.6	73.6
		10°	3.88	5.62	8.51	13.8	24.3	46.9

Source: After Caquot and Kerisel (1948).

considerably more accurate than those given by Rankine or Coulomb theory; the Rankine and Coulomb coefficient tend to underpredict and overpredict the maximum passive earth pressure, respectively. Rankine theory greatly underpredicts actual passive earth pressures and is rarely used for that purpose. Coulomb theory overpredicts passive pressures (an unconservative error) by about 11% for $\delta = \phi/2$ and by 100% or more for $\delta = \phi$. For that reason, Coulomb theory is rarely used to evaluate passive earth pressures when $\delta > \phi/2$.

11.4.4 Stress–Deformation Analysis

Since the actual pressures that act on retaining walls depend on interaction between the wall and the surrounding soil, it seems logical to expect that they could be estimated by stress–deformation techniques such as the finite-element method. Finite-element analyses are, in fact, very useful for estimating retaining wall pressures and movements (Clough and Duncan, 1971; Duncan et al., 1990). In addition, they can help explain unexpected or anomalous field measurements of actual wall behavior (Clough and Duncan, 1971; Duncan and Clough, 1971).

The accuracy of stress–deformation analyses, however, depends on how well they are able to model the actual field conditions. A useful method of analysis should be able to describe the stress–strain behavior of the soil (which is nonlinear) and wall (usually assumed to remain linear), the stress–displacement behavior of the soil–wall interface, and the sequence of wall construction and backfill placement. Without careful attention to each of these factors, the results of a finite-element analysis may have limited applicability.

11.5 DYNAMIC RESPONSE OF RETAINING WALLS

The dynamic response of even the simplest type of retaining wall is quite complex. Wall movements and pressures depend on the response of the soil underlying the wall, the response of the backfill, the inertial and flexural response of the wall itself, and the nature of the input motions. Since few well-documented case histories involving field measurements of wall response are available, most of the current understanding of the dynamic response of retaining walls has come from model tests and numerical analyses. These tests and analyses, the majority of which have involved gravity walls, indicate that:

1. Walls can move by translation and/or rotation. The relative amounts of translation and rotation depend on the design of the wall; one or the other may predominate for some walls (Nadim and Whitman, 1984), and both may occur for others (Siddharthan et al., 1992).
2. The magnitude and distribution of dynamic wall pressures are influenced by the mode of wall movement (e.g., translation, rotation about the base, or rotation about the top) (Sherif et al., 1982; Sherif and Fang, 1984a,b).
3. The maximum soil thrust acting on a wall generally occurs when the wall has translated or rotated *toward* the backfill (i.e., when the inertial force on the wall is directed toward the backfill). The minimum soil thrust occurs when the wall has translated or rotated *away* from the backfill.
4. The shape of the earth pressure distribution on the back of the wall changes as the wall moves. The point of application of the soil thrust therefore moves up and down along the back of the wall. The position of the soil thrust is highest when the wall has moved toward the soil and lowest when the wall moves outward.
5. Dynamic wall pressures are influenced by the dynamic response of the wall and backfill and can increase significantly near the natural frequency of the wall–backfill system (Steedman and Zeng, 1990). Permanent wall displacements also increase at frequencies near the natural frequency of the wall–backfill system (Nadim, 1982). Dynamic response effects can also cause deflections of different parts of the wall to be out of phase. This effect can be particularly significant for walls that penetrate into the foundation soils when the backfill soils move out of phase with the foundation soils.
6. Increased residual pressures may remain on the wall after an episode of strong shaking has ended (Whitman, 1990).

Given these complex, interacting phenomena and the inherent variability and uncertainty of soil properties, it is not currently possible to analyze all aspects of the seismic response of retaining walls accurately. As a result, simplified models that make various assumptions about the soil, structure, and input motion are most commonly used for seismic design of retaining walls.

11.6 SEISMIC PRESSURES ON RETAINING WALLS

One common approach to the seismic design of retaining walls involves estimating the loads imposed on the wall during earthquake shaking and then ensuring that the wall can

resist those loads. Because the actual loading on retaining walls during earthquakes is extremely complicated, seismic pressures on retaining walls are usually estimated using simplified methods.

11.6.1 Yielding Walls

Retaining walls that can move sufficiently to develop minimum active and/or maximum passive earth pressures are referred to as *yielding walls*. The dynamic pressures acting on yielding walls are usually estimated by pseudostatic procedures that share many features of those described for seismic slope stability analysis in Section 10.6.1.1. More recently, a pseudodynamic procedure that accounts, in an approximate manner, for the dynamic response of the backfill has been developed.

11.6.1.1 Mononobe–Okabe Method

Okabe (1926) and Mononobe and Matsuo (1929) developed the basis of a pseudostatic analysis of seismic earth pressures on retaining structures that has become popularly known as the Mononobe–Okabe (M-O) method. The M-O method is a direct extension of the static Coulomb theory to pseudostatic conditions. In a M-O analysis, pseudostatic accelerations are applied to a Coulomb active (or passive) wedge. The pseudostatic soil thrust is then obtained from force equilibrium of the wedge.

Active Earth Pressure Conditions. The forces acting on an active wedge in a dry, cohesionless backfill are shown in Figure 11.11a. In addition to the forces that exist under static conditions (Figure 11.7), the wedge is also acted upon by horizontal and vertical pseudostatic forces whose magnitudes are related to the mass of the wedge by the pseudostatic accelerations $a_h = k_h g$ and $a_v = k_v g$. The total active thrust can be expressed in a form similar to that developed for static conditions, that is,

$$P_{AE} = \tfrac{1}{2} K_{AE} \gamma H^2 (1 - k_v) \tag{11.15}$$

where the dynamic active earth pressure coefficient, K_{AE}, is given by

$$K_{AE} = \frac{\cos^2(\phi - \theta - \psi)}{\cos\psi \cos^2\theta \cos(\delta + \theta + \psi)\left[1 + \sqrt{\dfrac{\sin(\delta + \phi)\sin(\phi - \beta - \psi)}{\cos(\delta + \theta + \psi)\cos(\beta - \theta)}}\right]^2} \tag{11.16}$$

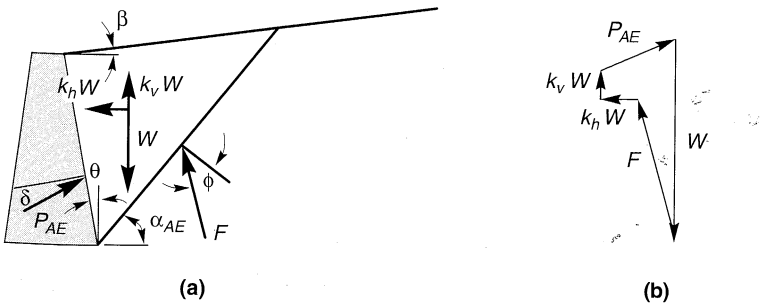

Figure 11.11 (a) Forces acting on active wedge in Mononobe–Okabe analysis, (b) force polygon illustrating equilibrium of forces acting on active wedge.

where $\phi - \beta \geq \psi$, $\gamma = \gamma_d$, and $\psi = \tan^{-1}[k_h/(1 - k_v)]$. The critical failure surface, which is flatter than the critical failure surface for static conditions, is inclined (Zarrabi-Kashani, 1979) at an angle

$$\alpha_{AE} = \phi - \psi + \tan^{-1}\left[\frac{-\tan(\phi - \psi - \beta) + C_{1E}}{C_{2E}}\right] \tag{11.17}$$

where

$$C_{1E} = \sqrt{\tan(\phi - \psi - \beta)\,[\tan(\phi - \psi - \beta) + \cot(\phi - \psi - \theta)]\,[1 + \tan(\delta + \psi + \theta)\cot(\phi - \psi - \theta)]}$$

$$C_{2E} = 1 + \{\tan(\delta + \psi + \theta)\,[\tan(\phi - \psi - \beta) + \cot(\phi - \psi - \theta)]\}$$

Although the M-O analysis implies that the total active thrust should act at a point $H/3$ above the base of a wall of height, H, experimental results suggest that it actually acts at a higher point under dynamic loading conditions. The total active thrust, P_{AE} [equation (11.15)], can be divided into a static component, P_A [equation (11.9)], and a dynamic component, ΔP_{AE}:

$$P_{AE} = P_A + \Delta P_{AE} \tag{11.18}$$

The static component is known to act at $H/3$ above the base of the wall. Seed and Whitman (1970) recommended that the dynamic component be taken to act at approximately $0.6H$. On this basis, the total active thrust will act at a height

$$h = \frac{P_A H/3 + \Delta P_{AE}(0.6H)}{P_{AE}} \tag{11.19}$$

above the base of the wall. The value of h depends on the relative magnitudes of P_A and P_{AE}—it often ends up near the midheight of the wall. M-O analyses show that k_v, when taken as one-half to two-thirds the value of k_h, affects P_{AE} by less than 10%. Seed and Whitman (1970) concluded that vertical accelerations can be ignored when the M-O method is used to estimate P_{AE} for typical wall designs.

Example 11.1

Compute the overturning moment about the base of the wall shown below for $k_h = 0.15$ and $k_v = 0.075$.

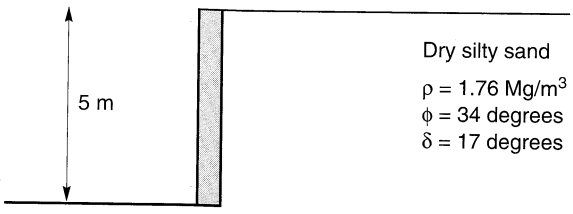

Figure E11.1

Solution First, estimate the static active thrust on the wall. Because the wall is not smooth ($\delta > 0$), Coulomb theory should be used. From equations (11.9) and (11.10),

$$K_A = \frac{\cos^2(34° - 0°)}{\cos^2(0°)\cos(17° + 0°)\left[1 + \sqrt{\dfrac{\sin(17° + 34°)\sin(34° - 0°)}{\cos(17° + 0°)\cos(0° - 0°)}}\right]^2} = 0.256$$

and

$$P_A = \frac{1}{2}K_A\gamma H^2 = \frac{1}{2}(0.256)(1.76\ \text{Mg/m}^3)(9.81\ \text{m/sec}^2)(5\ \text{m})^2 = 55.3\ \text{kN/m}$$

Now, the total active thrust can be computed from equations (11.15) and (11.16). The angle, ψ, is given by

$$\psi = \tan^{-1}\left(\frac{k_h}{1-k_v}\right) = \tan^{-1}\left(\frac{0.15}{1-0.075}\right) = 9.2°$$

and

$$K_{AE} = \frac{\cos^2(34° - 0° - 9.2°)}{\cos(9.2°)\cos^2(0°)\cos(17° + 0° + 9.2°)\left[1 + \sqrt{\dfrac{\sin(17° + 34°)\sin(34° + 0° - 9.2°)}{\cos(17° + 0° + 9.2°)\cos(0° - 0°)}}\right]^2}$$

$$= 0.362$$

and

$$P_{AE} = \frac{1}{2}K_{AE}\gamma H^2(1-k_v) = \frac{1}{2}(0.362)(1.76\ \text{Mg/m}^3)(9.81\ \text{m/sec}^2)(5\ \text{m})^2(1-0.075)$$

$$= 72.3\ \text{kN/m}$$

The dynamic component of the total thrust is

$$\Delta P_{AE} = P_{AE} - P_A = 72.3\ kN/\text{m} - 55.3\ \text{kN/m} = 17\ \text{kN/m}$$

From equation (11.19), the total thrust acts at a point

$$h = \frac{P_A\frac{H}{3} + \Delta P_{AE}(0.6H)}{P_{AE}} = \frac{55.3\ \text{kN/m}\ \frac{5\ \text{m}}{3} + 17\ \text{kN/m}(0.6)(5\ \text{m})}{72.3\ \text{kN/m}} = 1.98\ \text{m}$$

above the base of the wall. Because only the horizontal component of the total active thrust contributes to the overturning moment about the base, the overturning moment is given by

$$M_o = (P_{AE})_h\, h = (72.3\ \text{kN/m})\cos(17°)(1.98\ \text{m}) = 137\ \frac{\text{kN-m}}{\text{m}}$$

Passive Earth Pressure Conditions. The total passive thrust on a wall retaining a dry, cohesionless backfill (Figure 11.12) is given by

$$P_{PE} = \tfrac{1}{2}K_{PE}\gamma H^2(1-k_v) \tag{11.20}$$

where the dynamic passive earth pressure coefficient, K_{PE}, is given by

$$K_{PE} = \frac{\cos^2(\phi + \theta - \psi)}{\cos\psi\cos^2\theta\cos(\delta - \theta + \psi)\left[1 - \sqrt{\dfrac{\sin(\delta + \phi)\sin(\phi + \beta - \psi)}{\cos(\delta - \theta + \psi)\cos(\beta - \theta)}}\right]^2} \tag{11.21}$$

The critical failure surface for M-O passive conditions is inclined from horizontal by an angle

$$\alpha_{PE} = \psi - \phi + \tan^{-1}\left[\frac{\tan(\phi + \psi + \beta) + C_{3E}}{C_{4E}}\right] \tag{11.22}$$

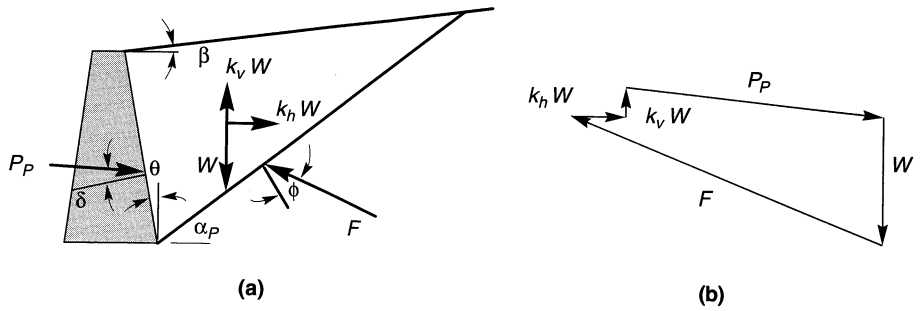

Figure 11.12 (a) Forces acting on passive wedge in Mononobe–Okabe analysis; (b) force polygon illustrating equilibrium of forces acting on passive wedge.

where

$$C_{3E} = \sqrt{\tan(\phi + \beta - \psi)\,[\tan(\phi + \beta - \psi) + \cot(\phi + \theta - \psi)]\,[1 + \tan(\delta + \psi - \theta)\cot(\phi + \theta - \psi)]}$$

$$C_{4E} = 1 + \{\tan(\delta + \psi - \theta)\,[\tan(\phi + \beta - \psi) + \cot(\phi + \theta - \psi)]\}$$

The total passive thrust can also be divided (Towhata and Islam, 1987) into static and dynamic components:

$$P_{PE} = P_P + \Delta P_{PE} \tag{11.23}$$

where P_{PE} and P_P are computed from equations (11.20) and (11.12), respectively. Note that the dynamic component acts in the opposite direction of the static component, thus reducing the available passive resistance.

Discussion. Although conceptually quite simple, the M-O analysis provides a useful means of estimating earthquake-induced loads on retaining walls. A positive horizontal acceleration coefficient causes the total active thrust to exceed the static active thrust and the total passive thrust to be less than the static passive thrust. Since the stability of a particular wall is generally reduced by an increase in active thrust and/or a decrease in passive thrust, the M-O method produces seismic loads that are more critical than the static loads that act prior to an earthquake. The effects of distributed and discrete surface loads and irregular backfill surfaces are easily considered by modifying the free-body diagram of the active or passive wedge. In such cases, equations (11.16) and (11.21) no longer apply—the total thrusts must be obtained from the analysis of a number of potential failure planes.

As a pseudostatic extension of the Coulomb analysis, however, the M-O analysis is subject to all of the limitations of pseudostatic analyses as well as the limitations of Coulomb theory. As in the case of pseudostatic slope stability analyses (Section 10.6.1.1), determination of the appropriate pseudostatic coefficient is difficult and the analysis is not appropriate for soils that experience significant loss of strength during earthquakes (e.g., liquefiable soils). Just as Coulomb theory does under static conditions, the M-O analysis will overpredict the actual total passive thrust, particularly for $\delta > \phi/2$. For these reasons the M-O method should be used and interpreted carefully.

11.6.1.2 Steedman–Zeng Method

As a pseudostatic analysis, the M-O method accounts for the dynamic nature of earthquake loading in a very approximate way. It is possible, however, to account for certain dynamic response characteristics in a relatively simple manner. To account for phase difference and amplification effects within the backfill behind a retaining wall can be considered using a simple pseudodynamic analysis of seismic earth pressures (Steedman and Zeng, 1990).

Consider the fixed-base cantilever wall shown in Figure 11.13. If the base is subjected to harmonic horizontal acceleration of amplitude a_h, the acceleration at a depth z, below the top of the wall can be expressed as

$$a(z, t) = a_h \sin\left[\omega\left(t - \frac{H - z}{v_s}\right)\right] \tag{11.24}$$

If the seismic wall pressures are assumed to result from the soil within a triangular wedge inclined at α to the horizontal, the mass of a thin element of the wedge at depth z is

$$m(z) = \frac{\gamma}{g}\frac{H - z}{\tan\alpha}dz \tag{11.25}$$

where γ is the unit weight of the backfill. The total inertial force acting on the wall can therefore be expressed as

$$Q_h(t) = \int_0^H m(z)a(z, t)dz = \frac{\lambda\gamma a_h}{4\pi^2 g \tan\alpha}[2\pi H \cos\omega\zeta + \lambda(\sin\omega\zeta - \sin\omega t)] \tag{11.26}$$

where $\lambda = 2\pi v_s/\omega$ is the wavelength of the vertically propagating shear wave and $\zeta = t - H/v_s$. The special case of a rigid wedge is given, in the limit, as

$$\lim_{v_S \to \infty}(Q_h)_{\max} = \frac{\gamma H^2 a_h}{2g \tan\alpha} = \frac{a_h}{g}W = k_h W \tag{11.27}$$

which is equivalent to the pseudostatic force assumed by the M-O method. The total (static plus dynamic) soil thrust can be obtained by resolving forces on the wedge, that is,

$$P_{AE}(t) = \frac{Q_h(t)\cos(\alpha - \phi) + W\sin(\alpha - \phi)}{\cos(\delta + \phi - \alpha)} \tag{11.28}$$

and the total earth pressure distribution by differentiating the total soil thrust

$$p_{AE}(t) = \frac{\partial P_{AE}(t)}{\partial z} = \frac{\gamma z}{\tan\alpha}\frac{\sin(\alpha - \phi)}{\cos(\delta + \phi - \alpha)} + \frac{k_h\gamma z}{\tan\alpha}\frac{\cos(\alpha - \phi)}{\cos(\delta + \phi - \alpha)}\sin\left[\omega\left(t - \frac{z}{v_s}\right)\right] \tag{11.29}$$

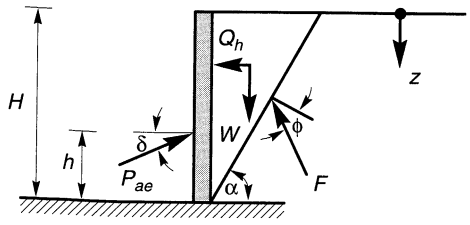

Figure 11.13 Wall geometry and notation for Steedman–Zeng method.

The first term in equation (11.29), which increases linearly with depth and does not vary with time, represents the static earth pressure acting on the wall. The resultant static thrust acts in accordance with static earth pressure theories at a point $h_s = H/3$ above the base of the wall. The second term represents the dynamic earth pressure. It increases as a nonlinear function of depth with a shape that depends on the ratio H/λ. A typical example of the nonlinear dynamic pressure is shown in Figure 11.14. Since the dynamic pressure increases nonlinearly with depth, the position of the dynamic thrust varies with time according to

$$h_d = H - \frac{2\pi^2 H^2 \cos\,\omega\zeta + 2\pi\lambda H \sin\,\omega\zeta - \lambda^2(\cos\,\omega\zeta - \cos\,\omega t)}{2\pi H \cos\,\omega\zeta + \pi\lambda(\sin\,\omega\zeta - \sin\,\omega t)} \tag{11.30}$$

The point of application of the dynamic thrust for very low frequency motions (small H/λ, so the backfill moves essentially in phase) is at $h_d = H/3$. For higher-frequency motions, the point of application moves higher on the wall, as indicated in Figure 11.15.

Steedman and Zeng (1989) found that the soil thrusts for backfills of different stiffnesses were close to those obtained when the mean shear wave velocities of the backfill were used in the pseudodynamic analyses. Backfill amplification effects can also be considered by expressing a_h as a function of depth [rather than as a constant in equation (11.24)] and repeating the integration of equation (11.26). Note that backfill amplification will increase both the loads acting on the wall and the height of the resultant soil thrust. Assuming that $a_h(z, t)$ varied linearly from the input acceleration at the base of the wall to a value twice as large at the top, Steedman and Zeng (1990) showed good agreement with the results of centrifuge tests.

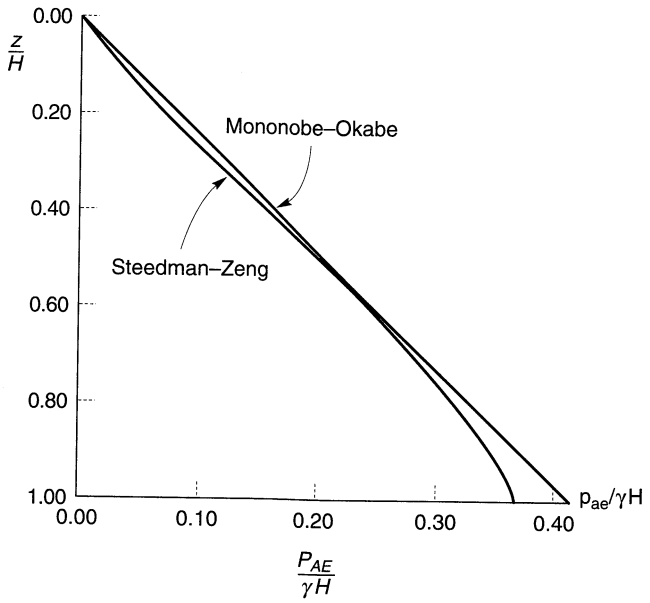

Figure 11.14 Comparison of normalized pressure distributions for M-O and Steedman–Zeng methods assuming that $k_h = 0.2$ and $H/\lambda = 0.3$. (After Steedman and Zeng, 1990.)

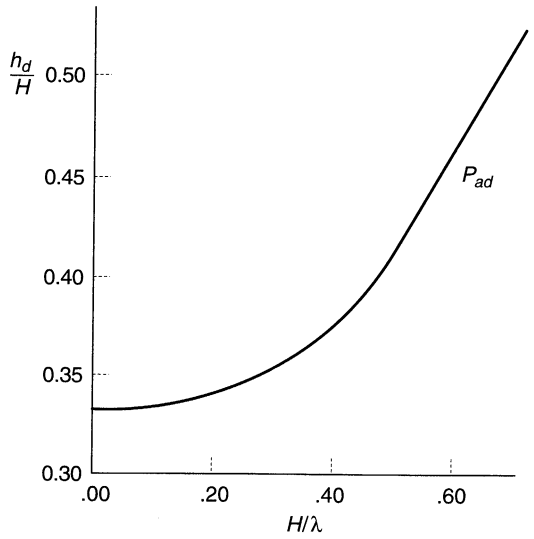

Figure 11.15 Location of dynamic thrust at instant of maximum overturning moment for $k_h = 0.2$. (After Steedman and Zeng, 1990.)

11.6.2 Nonyielding Walls

Some retaining structures, such as massive gravity walls founded on rock or basement walls braced at both top and bottom, do not move sufficiently to mobilize the shear strength of the backfill soil. As a result, the limiting conditions of minimum active or maximum passive earth pressures cannot be developed.

Wood (1973) analyzed the response of a homogeneous linear elastic soil trapped between two rigid walls connected to a rigid base (Figure 11.16). If the two walls are assumed to be spaced far apart, the pressures on one wall will not be strongly influenced by the presence of the other. Wood showed that dynamic amplification was negligible for low-frequency input motions [i.e., motions at less than half the fundamental frequency of the unrestrained backfill ($f_o = v_s/4H$)]. For this range of frequencies, in which many practical problems lie, wall pressures can be obtained from the elastic solution for the case of a uniform, constant, horizontal acceleration applied throughout the soil. For smooth rigid walls, Wood (1973) expressed the dynamic thrust and dynamic overturning moment (about the base of the wall) in the form

$$\Delta P_{\text{eq}} = \gamma H^2 \frac{a_h}{g} F_p \tag{11.31}$$

$$\Delta M_{\text{eq}} = \gamma H^3 \frac{a_h}{g} F_m \tag{11.32}$$

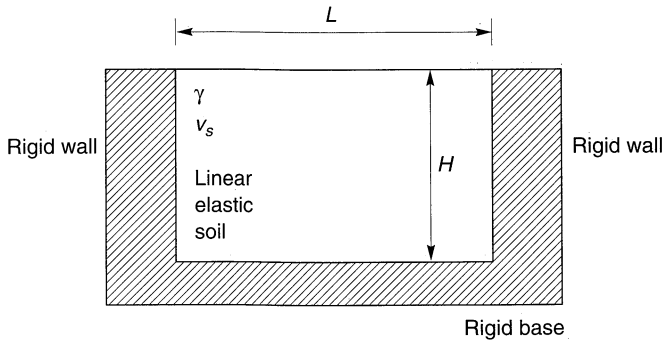

Figure 11.16 Wall geometry and notation for Wood (1973) analysis of pressures on nonyielding walls.

where a_h is the amplitude of the harmonic base acceleration and F_p and F_m are the dimensionless dynamic thrust and moment factors shown in Figures 11.17 and 11.18, respectively. The point of application of the dynamic thrust is at a height

$$h_{eq} = \frac{\Delta M_{eq}}{\Delta P_{eq}} \tag{11.33}$$

above the base of the wall; typically, $h_{eq} \approx 0.63H$.

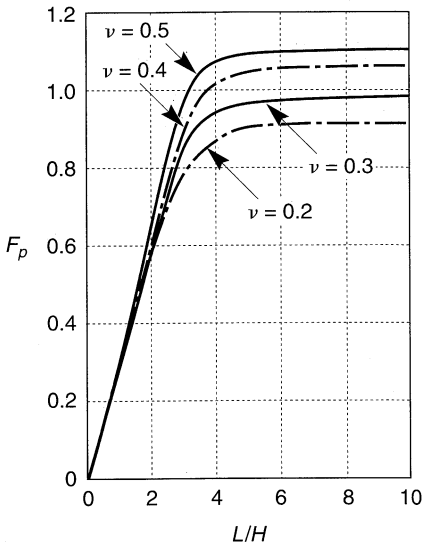

Figure 11.17 Dimensionless thrust factor for various geometries and soil Poisson's ratio values. After Wood (1973).

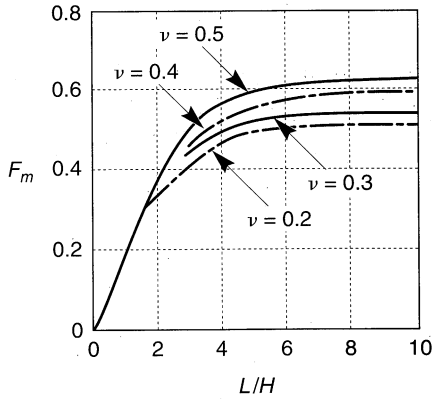

Figure 11.18 Dimensionless moment factor for various geometries and soil Poisson's ratio values. After Wood (1973).

Example 11.2

A reinforced concrete box culvert is used to provide an undercrossing through a railroad embankment as shown below. Estimate the dynamic thrust on a wall of the culvert when subjected to a ground motion with $k_h = 0.2$.

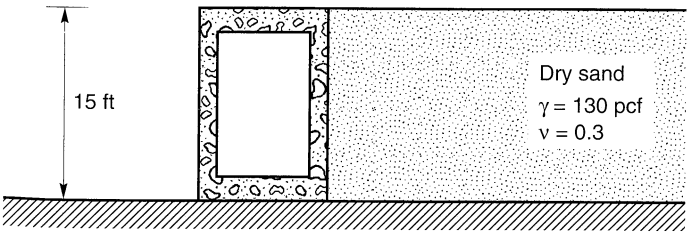

Figure E11.2

Solution Assuming they are properly reinforced and that the culvert cannot slide on its base, the culvert walls will not yield. Consequently, the dynamic thrust can be estimated using equation (11.31) and Figure 11.17

$$\Delta P_{eq} = \gamma H^2 \frac{a_h}{g} F_p = (130 \text{ pcf})(15 \text{ ft})^2 \frac{0.2\ g}{g}(1.0) = 5850 \text{ lb/ft}$$

11.6.3 Effects of Water on Wall Pressures

The procedures for estimation of seismic loads on retaining walls described in the preceding sections have been limited to cases of dry backfills. Most retaining walls are designed with drains to prevent water from building up within the backfill. This is not possible, however, for retaining walls in waterfront areas, where most earthquake-induced wall failures have been observed.

The presence of water plays a strong role in determining the loads on waterfront retaining walls both during and after earthquakes. Water outboard of a retaining wall can exert dynamic pressures on the face of the wall. Water within a backfill can also affect the dynamic pressures that act on the back of the wall. Proper consideration of the effects of water is essential for the seismic design of retaining structures, particularly in waterfront areas. Since few waterfront retaining structures are completely impermeable, the water level in the backfill is usually at approximately the same level as the free water outboard of the wall. Backfill water levels generally lag behind changes in outboard water level—the difference in water level depends on the permeability of the wall and backfill and on the rate at which the outboard water level changes. The total water pressures that act on retaining walls in the absence of seepage within the backfill can be divided into two components: *hydrostatic pressure*, which increases linearly with depth and acts on the wall before, during, and after earthquake shaking, and *hydrodynamic pressure*, which results from the dynamic response of the water itself.

11.6.3.1 Water Outboard of Wall

Hydrodynamic water pressure results from the dynamic response of a body of water. For retaining walls, hydrodynamic pressures are usually estimated from Westergaard's

solution (Westergaard, 1931) for the case of a vertical, rigid dam retaining a semi-infinite reservoir of water that is excited by harmonic, horizontal motion of its rigid base. Westergaard showed that the hydrodynamic pressure amplitude increased with the square root of water depth when the motion is at applied at a frequency lower than the fundamental frequency of the reservoir, $f_o = v_p/4H$, where v_p is the p-wave velocity of water (about 4700 ft/sec (1400 m/sec)) and H is the depth of water in the reservoir (the natural frequency of a 20-ft-deep (6.1 m) reservoir, for example, would be over 58 Hz, well above the frequencies of interest for earthquakes). Westergaard computed the amplitude of the hydrodynamic pressure as

$$p_w = \frac{7}{8}\frac{a_h}{g}\gamma_w\sqrt{z_w H} \tag{11.34}$$

The resultant hydrodynamic thrust is given by

$$P_w = \frac{7}{12}\frac{a_h}{g}\gamma_w H^2 \tag{11.35}$$

The total water pressure on the face of the wall is the sum of the hydrostatic and hydrodynamic water pressures. Similarly, the total lateral thrust due to the water is equal to the sum of the hydrostatic and hydrodynamic thrusts.

Another important consideration in the design of a waterfront retaining wall is the potential for rapid drawdown of the water outboard of the wall. Earthquakes occurring near large bodies of water often induce long-period motion of the water, such as tsunamis or seiches (Section 1.4.7), that cause the water surface to move up and down. While the upward movement of water outboard of a retaining wall will generally tend to stabilize the wall (assuming that it does not rise above the level of the top of the wall), downward movement can create a destabilizing rapid drawdown condition. When liquefiable soils exist under relatively high levels of initial shear stress, failures can be triggered by very small changes in water level. Such failures can originate in the soils adjacent to or beneath the retaining structure rather than in the backfill.

11.6.3.2 Water in Backfill

The presence of water in the backfill behind a retaining wall can influence the seismic loads that act on the wall in three ways: (1) by altering the inertial forces within the backfill, (2) by developing hydrodynamic pressures within the backfill, and (3) by allowing excess porewater pressure generation due to cyclic straining of the backfill soils.

The inertial forces in saturated soils depend on the relative movement between the backfill soil particles and the porewater that surrounds them. If, as is usually the case, the permeability of the soil is small enough (typically $k \leq 10^{-3}$ cm/sec (33×10^{-5} ft/sec) or so) that the porewater moves with the soil during earthquake shaking (no relative movement of soil and water, or *restrained porewater conditions*), the inertial forces will be proportional to the *total* unit weight of the soil. If the permeability of the backfill soil is very high, however, the porewater may remain essentially stationary while the soil skeleton moves back and forth (the soil particles move through the porewater in *free porewater conditions*). In such cases, inertial forces will be proportional to the *buoyant* (or submerged) unit weight of the soil. Hydrodynamic water pressures (Section 11.5.3.1) can also develop under free

pore-water conditions and must be added to the computed soil and hydrostatic pressures to obtain the total loading on the wall.

For restrained porewater conditions, the M-O method can be modified to account for the presence of porewater within the backfill (Matsuzawa et al., 1985). Representing the excess porewater pressure in the backfill by the pore pressure ratio, r_u (Section 9.5.1.1), the active soil thrust acting on a yielding wall can be computed from equation (11.15) using

$$\gamma = \gamma_b(1 - r_u) \tag{11.36}$$

$$\psi = \tan^{-1}\left[\frac{\gamma_{sat}k_h}{\gamma_b(1 - r_u)(1 - k_v)}\right] \tag{11.37}$$

An equivalent hydrostatic thrust based on a fluid of unit weight $\gamma_{eq} = \gamma_w + r_u\gamma_b$ must be added to the soil thrust. Note that as r_u approaches 1 (as it could in a liquefiable backfill), the wall thrust approaches that imposed by a fluid of equivalent unit weight, $\gamma_{eq} = \gamma_{sat}$. As discussed in Chapter 9, subsequent unidirectional movement of a soil that develops high excess porewater pressures may, depending on its residual (or steady state) strength, cause dilation with accompanying porewater pressure reduction and strength gain.

Soil thrusts from partially submerged backfills may be computed using an average unit weight based on the relative volumes of soil within the active wedge that are above and below the phreatic surface (Figure 11.19):

$$\bar{\gamma} = \lambda^2\gamma_{sat} + (1 - \lambda^2)\gamma_d \tag{11.38}$$

Again, the hydrostatic thrust (and hydrodynamic thrust, if present) must be added to the soil thrust.

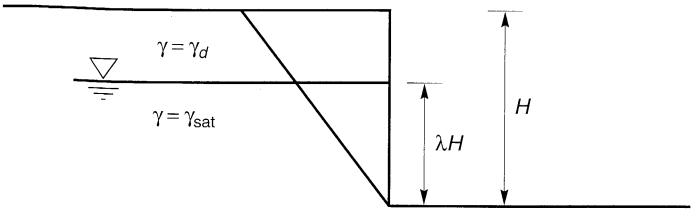

Figure 11.19 Geometry and notation for partially submerged backfill.

Example 11.3

Compute the total thrust that would be expected on the wall shown in Example 11.1 if the wall backfill was completely saturated. Assume that the pore pressure ratio, r_u, reaches a value of 0.5.

Solution The total active thrust can be computed from equation (11.15) using

$$\gamma = \gamma_b(1 - r_u) = \rho_b g(1 - r_u) = \frac{G_s - 1}{G_s}\rho_d g(1 - r_u)$$

$$= \frac{2.65 - 1}{2.65}(1.76\ \text{Mg/m}^3)(9.81\ \text{m/sec}^2)(1 - 0.5) = 5.44\ \text{kN/m}^3$$

$$\psi = \tan^{-1}\left[\frac{\gamma_{sat}k_h}{\gamma_b(1 - r_u)(1 - k_v)}\right] = \tan^{-1}\left[\frac{(10.9\ \text{kN/m}^3 + 9.8\ \text{kN/m}^3)(0.15)}{(10.9\ \text{kN/m}^3)(1 - 0.5)(1 - 0.075)}\right] = 31.6°$$

Then

$$K_{AE} = \frac{\cos^2(34° - 0° - 31.6°)}{\cos(31.6°)\cos(0°)\cos(17° + 0° + 31.6°)\left[1 + \sqrt{\frac{\sin(17° + 31.6°)\sin(34° - 0° - 31.6°)}{\cos(17° + 0° + 31.6°)\cos(0° - 0°)}}\right]^2}$$

$$= 1.195$$

and

$$P_{AE} = \frac{1}{2}K_{AE}\gamma H^2(1 - k_v) = \frac{1}{2}(1.195)(5.44 \text{ kN/m}^3)(5 \text{ m})^2(1 - 0.075) = 75.2 \text{ kN/m}$$

The hydrostatic thrust is given by

$$P_w = \frac{1}{2}\gamma_{eq}H^2 = \frac{1}{2}(\gamma_w + r_u\gamma_b)H^2 = \frac{1}{2}[9.81 \text{ kN/m}^3 + (0.5)(10.9 \text{ kN/m}^3)](5 \text{ m})^2$$

$$= 190.6 \text{ kN/m}$$

Therefore, the total thrust is

$$P_{tot} = P_{AE} + P_w = 75.2 \text{ kN/m} + 190.6 \text{ kN/m} = 265.8 \text{ kN/m}$$

11.6.4 Finite-Element Analysis

Earthquake-induced pressures on retaining walls can also be evaluated using dynamic response–analyses. A number of computer programs are available for such analyses (Section 7.3). Linear or equivalent linear analyses can be used to estimate wall pressures, although their inability to represent actual modes of failure can make their results difficult to interpret. Nonlinear analyses are capable of predicting permanent deformations (Section 11.6.3) as well as wall pressures.

11.7 SEISMIC DISPLACEMENTS OF RETAINING WALLS

Although the methods of analysis described in the preceding section provide useful information on the seismic loads that act on retaining walls, the postearthquake serviceability of such walls is more closely related to the permanent deformations that occur during earthquakes. While large permanent deformations may be acceptable for some walls, others may be considered to have failed at much smaller deformations. Analyses that predict permanent wall deformations may provide a more useful indication of retaining wall performance. Several methods have been proposed for predicting permanent deformations of yielding walls.

11.7.1 Richards–Elms Method

Richards and Elms (1979) proposed a method for the seismic design of gravity walls based on allowable permanent wall displacements. The method estimates permanent displacements in a manner analogous to the Newmark sliding block procedure (Section 10.6.1.2) developed originally for evaluation of seismic slope stability.

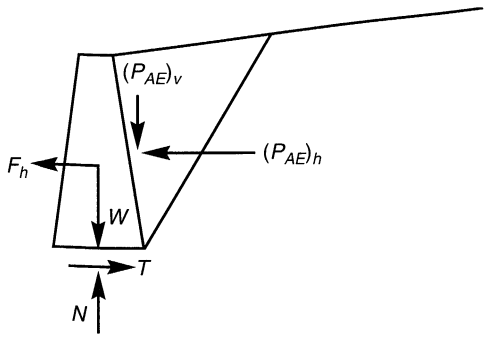

Figure 11.20 Gravity wall acted upon by gravity and pseudostatic accelerations.

Application of the Richards–Elms method requires evaluation of the yield acceleration for the wall–backfill system. Consider the gravity wall shown in Figure 11.20. When the active wedge is subjected to acceleration acting toward the backfill, the resulting inertial forces will act away from the backfill. The level of acceleration that is just large enough to cause the wall to slide on its base is the *yield acceleration*. When the acceleration is equal to the yield acceleration, horizontal and vertical equilibrium require that

$$\begin{aligned} T &= F_h + (P_{AE})_h \\ N &= W + (P_{AE})_v \end{aligned} \tag{11.39}$$

Substituting $T = N \tan \phi_b$, $F_h = a_y W/g$, $(P_{AE})_h = P_{AE} \cos(\delta + \theta)$, and $(P_{AE})_v = P_{AE} \sin(\delta + \theta)$, the yield acceleration can be computed as

$$a_y = \left[\tan \phi_b - \frac{P_{AE} \cos(\delta + \theta) - P_{AE} \sin(\delta + \theta)}{W}\right] g \tag{11.40}$$

Richards and Elms recommended that P_{AE} be calculated using the M-O method (since the M-O method requires that a_y be known, the solution of equation (11.40) must be obtained iteratively). Using the results of sliding block analyses in the same manner as Newmark (1965) and Franklin and Chang (1977), Richards and Elms proposed the following expression for permanent block displacement:

$$d_{\text{perm}} = 0.087 \frac{v_{\max}^2 a_{\max}^3}{a_y^4} \qquad \frac{a_y}{a_{\max}} \geq 0.3 \tag{11.41}$$

where $v_{\max}$ is the peak ground velocity, $a_{\max}$ the peak ground acceleration, and a_y the yield acceleration for the wall–backfill system. Equation (11.41) provides displacement estimates that are close to the estimated maximum displacements [equation (10.13)] of Newmark (1965).

Example 11.4

Estimate the permanent displacement of the concrete gravity wall shown below that would be produced by the Gilroy No. 2 (soil) motion. Assume $k_v = 0$.

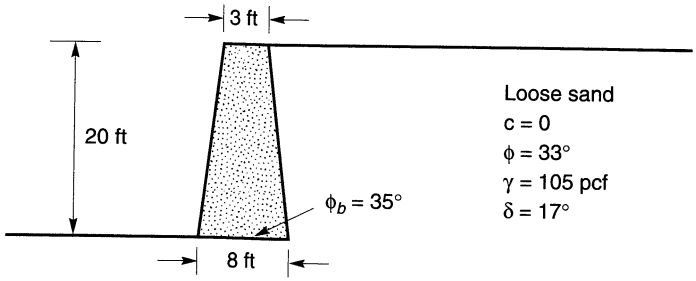

Figure E11.4

Solution The weight of the wall section is

$$W = (20 \text{ ft})\left(\frac{8 \text{ ft} + 3 \text{ ft}}{2}\right)(150 \text{ lb/ft}^3) = 16500 \text{ lb/ft}$$

The total active thrust can be estimated by the Mononobe–Okabe approach. From equations (11.15) and (11.16). Assuming a trial pseudostatic acceleration of $0.10g$, $\psi = 5.7°$ and

$$K_{AE} = \frac{\cos^2(33° - 7.1° - 5.7°)}{\cos(5.7°)\cos^2(7.1°)\cos(17° + 7.1° + 5.7°)\left[1 + \sqrt{\dfrac{\sin(17° + 33°)\sin(33° - 0° - 5.7°)}{\cos(17° + 7.1° + 5.7°)\cos(0° - 7.1°)}}\right]^2}$$

$$= 0.385$$

and

$$P_{AE} = \frac{1}{2}(0.385)(105 \text{ pcf})(20 \text{ ft})^2 = 8085 \text{ lb/ft}$$

Then, from equation (11.40),

$$a_y = \left[\tan(35°) - \frac{(8085 \text{ lb/ft})\cos(17 + 7.1) - (8085 \text{ lb/ft})\sin(17 + 7.1)}{16500 \text{ lb/ft}}\right]g = 0.45g$$

Because the computed yield acceleration ($0.43g$) is inconsistent with the assumed pseudostatic acceleration ($0.10g$), another iteration is required. For the next iteration, assume that the pseudostatic acceleration is $0.30g$. Then ψ is 16.7° and

$$K_{AE} = \frac{\cos^2(33° - 7.1° - 16.7°)}{\cos(16.7°)\cos^2(7.1°)\cos(17° + 7.1° + 16.7°)\left[1 + \sqrt{\dfrac{\sin(17° + 33°)\sin(33° - 0° - 16.7°)}{\cos(17° + 7.1° + 16.7°)\cos(0° - 7.1°)}}\right]^2}$$

$$= 0.574$$

and

$$P_{AE} = \frac{1}{2}(0.574)(105 \text{ pcf})(20 \text{ ft})^2 = 12054 \text{ lb/ft}$$

Then, from equation (11.40),

$$a_y = \left[\tan(35°) - \frac{(12054 \text{ lb/ft})\cos(17 + 7.1) - (12054 \text{ lb/ft})\sin(17 + 7.1)}{16500 \text{ lb/ft}}\right] g = 0.33\text{g}$$

Now, the computed yield acceleration is fairly close to the assumed pseudostatic acceleration. Using equation (11.41) with the results of Example 3.1

$$d_{\text{perm}} = 0.087\frac{(39.2 \text{ cm/sec})^2 [(0.322g)(981 \text{ cm/sec}^2/\text{g})]^3}{[(0.30g)(981 \text{ cm/sec}^2/\text{g})]^4} = 6.5\text{cm}$$

11.7.2 Whitman–Liao Method

The Richards–Elms method offers a rational deterministic approach to the estimation of gravity wall displacements. Its simplicity comes, in part, from assumptions that neglect certain aspects of the dynamic earth pressure problem. Whitman and Liao (1985) identified several modeling errors that result from the simplifying assumptions of the Richards–Elms procedure. The most important of these are neglect of the dynamic response of the backfill, neglect of kinematic factors, neglect of tilting mechanisms, and neglect of vertical accelerations. Finite-element analyses of the effects of the dynamic response of the backfill on wall displacements (Nadim, 1982), for example, show that amplification occurs when input motions coincide with the natural period of the backfill and produce considerably greater permanent displacement than the rigid-block model used by Richards and Elms. Analyses in which the backfill wedge and wall were treated as separate blocks (Zarrabi-Kashani, 1979) show that the kinematic requirements of horizontal *and* vertical displacement of the backfill wedge cause systematically smaller displacements than the single-block model of Richards and Elms. Studies of combined tilting and sliding (Nadim, 1980; Siddharthan et al., 1992), indicate that tilting mechanisms generally increase wall displacements over those produced by sliding-only models such as that of Richards and Elms. Consideration of vertical accelerations produces slightly larger displacements than when they are neglected, at least for motions with high peak horizontal acceleration ($a_{\max}$ greater than about $0.5g$) and $a_y/a_{\max} \geq 0.4$ (Whitman and Liao, 1985). Whitman and Liao quantified and combined the effects of each of these sources of modeling error to describe the total modeling error by a lognormally distributed random variable with mean value, $\overline{M}$, and standard deviation, $\sigma_{\ln M}$.

Using the results of sliding block analyses of 14 ground motions by Wong (1982), Whitman and Liao found that the permanent displacements were lognormally distributed with mean value

$$\overline{d}_{\text{perm}} = \frac{37 v_{\max}^2}{a_{\max}} \exp\left(\frac{-9.4\, a_y}{a_{\max}}\right) \tag{11.42}$$

Uncertainty due to statistical variability of ground motions was characterized by a lognormally distributed random variable, Q, with a mean value of $\overline{Q}$ and standard deviation, $\sigma_{\ln Q}$.

The effects of uncertainty in soil properties, specifically the friction angles, on permanent displacement were also investigated. Using standard deviations of $\sigma_\phi = 2$ to $3°$ for soil friction angles and $\sigma_\delta = 5°$ for wall–soil interface friction angles, the computed yield acceleration [the only term on the right side of equation (11.40) that is a function of ϕ and

δ] was defined as a random variable with mean value $\bar{a}_y$ and standard deviation σ_{a_y}. The mean value $\bar{a}_y$ is the yield acceleration computed using the mean values of ϕ and δ.

Combining all of these sources of uncertainty, the permanent displacement can be characterized as a lognormally distributed random variable with mean value

$$\bar{d} = \frac{37 v_{\max}^2}{a_{\max}} \exp\left(\frac{-9.4\,\bar{a}_y}{a_{\max}}\right) \bar{Q}\bar{M} \tag{11.43}$$

and variance

$$\sigma_{\ln d}^2 = \left(\frac{9.4g}{a_{\max}}\right)^2 \sigma_{a_y}^2 + \sigma_{\ln M}^2 + \sigma_{\ln Q}^2 \tag{11.44}$$

Suggested values of the means and standard deviations of the ground motion, soil resistance, and model error factors are shown in Table 11-4.

Table 11-4 Mean and Standard Deviation Values for Gravity Wall Displacement Analysis

Factor	Mean	Standard Deviation
Model error	$\bar{M} = 3.5$	$\sigma_{\ln M} = 0.84$
Soil resistance	$\bar{a_y} = a_y(\bar{\phi}, \bar{\delta})$	$\sigma_{a_y} = 0.04$ to 0.065
Ground motion	$\bar{Q} = 1$	$\sigma_{\ln Q} = 0.58$ to 1.05

Source: After Whitman and Liao (1985).

Using equations (11.43) and (11.44), along with the CDF for the standard normal variable (Table C-1), the probability of exceeding any particular value of d_{all} can easily be computed.

Example 11.5

Estimate the expected permanent displacement of the gravity wall shown in Example 11.4 using the Whitman–Liao approach.

Solution From equation (11.42), the mean or expected value of permanent displacement is given by

$$d_{\text{perm}} = 37 \frac{(39.2 \text{ cm/sec})^2}{[\,(0.322g)\,(981 \text{ cm/sec}^2/\text{g})]} \exp\,[(-9.4)(0.30g)/0.322g] = 0.03 \text{ cm}$$

Note that the mean permanent displacement is considerably smaller than the displacement predicted by the Richards–Elms method in Example 11.4.

11.7.3 Finite-Element Analysis

Earthquake-induced deformations of retaining walls can be predicted by dynamic stress–deformation analyses. Obviously, prediction of permanent deformations requires the use of a nonlinear analysis (Section 7.2.3). A rigorous analysis should be capable of accounting for nonlinear, inelastic behavior of the soil and of the interfaces between the soil and wall elements. Among the relatively few examples of rigorous two-dimensional finite-element analyses that predict permanent deformations are those reported by Alampalli and Elgamel (1990), Finn et al. (1992), and Iai and Kameoka (1993).

11.8 SEISMIC DESIGN CONSIDERATIONS

The design of retaining walls for seismic conditions is similar, in many respects, to designing for static conditions. In both cases, potential modes of failure are identified and the wall designed to avoid initiating them. Although the response of retaining walls under seismic loading conditions is much more complex than under static conditions, conventional design procedures make use of simplifying assumptions that render the problem tractable. Several design approaches for different types of retaining walls are described in the following sections.

11.8.1 Gravity Walls

Gravity walls are the simplest type of retaining wall, and more attention has been paid to their design than to the design of other types of walls. Gravity wall design procedures, however, are commonly adapted as part of the design of cantilever walls and composite wall systems. Gravity walls are customarily designed by one of two approaches: a seismic pressure-based approach or a permanent displacement-based approach. Although the gravity wall design procedures are oriented toward prevention of sliding failure, the possibility of overturning due to bearing failure of the soil beneath the base of a wall must also be considered in design.

11.8.1.1 Design Based on Seismic Pressures

Gravity walls have traditionally been designed on the basis of seismic earth pressures. The M-O method is most commonly used along with an inertial force, using the same pseudostatic acceleration applied to the active wedge, applied to the wall itself. Pseudostatic accelerations are generally considerably smaller than anticipated peak accelerations. Values between $0.05g$ and $0.15g$, corresponding to one-third to one-half of the peak ground surface acceleration, are commonly used with factors of safety of 1.0 to 1.2 (Whitman, 1990).

Despite the considerable simplification of their complex actual behavior, gravity walls designed by the traditional approach have generally performed quite well in earthquakes. The reason, however, may have more to do with the conservatism commonly used in static wall design than with the accuracy of the M-O method. Design pressures that account for backfill amplification, such as those that can be obtained by the Steedman–Zeng method, should be considered for design of unusually tall or unusually displacement-sensitive walls.

11.8.1.2 Design Based on Allowable Displacements

Gravity walls are being designed on the basis of allowable displacements more and more frequently. This approach allows the designer to consider the consequences of permanent displacement for an individual wall when selecting an allowable displacement for design. Design procedures based on the Richards–Elms and Whitman–Liao procedures for estimation of permanent displacement are available.

The Richards–Elms design procedure involves calculation of the wall weight that would be required to ensure that permanent displacements are less than or equal to some allowable value. The procedure can be summarized as follows:

1. Select an allowable permanent displacement, d_{all}.
2. Calculate the yield acceleration required to produce the allowable permanent displacement from equation (11.41), rearranged in the form

$$a_y = \left(\frac{0.087 v_{max}^2 a_{max}^3}{d_{all}} \right)^{1/4} \tag{11.45}$$

3. Calculate P_{AE} using the M-O method with the yield acceleration from step 2 as the pseudostatic acceleration. This represents the soil thrust that would be expected to cause a maximum permanent displacement equal to d_{all}.
4. Calculate the wall weight required to limit the permanent displacement to the allowable permanent displacement using equation (11.40) rearranged in the form

$$W = \frac{P_{AE}\cos(\delta + \theta) - P_{AE}\sin(\delta + \theta)\tan \phi_b}{\tan \phi_b - a_y/g} \tag{11.46}$$

5. Apply a factor of safety to the weight of the wall. Richards and Elms originally suggested a factor of safety of 1.5, but subsequent research has shown that a wall weight factor of safety of 1.1 to 1.2 should be sufficient to reduce the probability of exceeding the allowable permanent displacement to 5% or less (Whitman and Liao, 1985).

Using the Whitman–Liao approach, gravity walls can be designed on the basis of allowable displacements that have defined probabilities of exceedance. The selection of an acceptable probability of exceedance is a complicated matter that may depend on the importance of the wall, the effects of failure, the cost of repair, and other technical and/or nontechnical factors. The actual wall design is accomplished by using equation (11.43) to compute the yield acceleration as

$$a_y = \frac{a_{max}}{9.4} \ln \frac{37 \bar{M} v_{max}^2}{a_{max} d_{all}} \tag{11.47}$$

and then using the M-O method to size the wall to meet or exceed the computed yield acceleration. Whitman and Liao suggest a conservative design (corresponding to a probability of exceedance of about 5%) can be obtained by assuming $d_{all} = 4\bar{d}_{perm}$, where $\bar{d}_{perm}$ is calculated from equation (11.42). A less conservative design (corresponding to about 10% probability of exceedance) is obtained by taking $d_{all} = 2.5\bar{d}_{perm}$.

11.8.2 Cantilever Walls

Cantilever walls are designed in much the same way as gravity walls, except that bending failure must also be considered. Maximum bending moments are usually calculated using the M-O method to compute the maximum soil thrust, which is taken to act at the height given by equation (11.19). The maximum overturning moment is used for structural design of wall elements (to prevent flexural failure of the wall itself) and to determine the size of the wall footing required to prevent bearing failure of the supporting soils.

11.8.3 Braced Walls

Because their lateral displacements are constrained by bracing elements, braced walls do not develop minimum active (or maximum passive) earth pressures in the vicinity of the

bracing elements. The earth pressures that do develop depend on the stiffness of the brace and the relative stiffness of the wall and soil. Analysis of actual soil–wall–brace interaction is quite complicated, and simplified methods are generally adopted for design purposes.

11.8.3.1 Non-Yielding Braced Walls

Walls that are braced sufficiently that they do not move at all, such as braced walls founded on rock, are usually designed to resist the earth pressures predicted by Wood's (1973) analysis. To avoid cracking or yielding of such walls, design pressures are usually based on the peak acceleration (Whitman, 1991). This approach, however, can lead to very high design pressures and some data [e.g., Chang et al. (1990)], indicates that the pressures on braced walls that can move slightly are lower. Dynamic finite-element analyses of stiff, embedded basement walls suggest that the M-O method with the peak ground surface acceleration outside the structure produces reasonable design earth pressures (Whitman, 1990).

Specifications for design of bridge abutments (e.g., AASHTO, 1991) recommend that nonyielding abutments be designed to resist lateral thrust obtained from the M-O method with a pseudostatic horizontal acceleration 50% greater than the effective peak acceleration.

11.8.3.2 Flexible Braced Walls

The seismic response of flexible braced walls such as anchored bulkheads and tieback walls is particularly complicated. Again, these complexities require that simplified methods be used for design. Because these types of walls are very commonly used in waterfront areas, and because the great majority of earthquake-induced retaining wall failures occur in waterfront areas, special attention to their design is required. In the case of anchored bulkheads, the simplified design procedures can be supplemented by a useful empirical model of damage potential based on observations of actual wall performance.

Anchored Bulkheads. The design of anchored bulkheads in waterfront areas is strongly influenced by liquefaction hazards. If widespread liquefaction occurs, experience indicates that bulkhead failures are very likely. Consequently, steps should be taken prior to construction to ensure that such liquefaction will not occur. Permanent seaward movements of anchored bulkheads in the absence of widespread liquefaction, however, has also been observed. Conventional design procedures seek to minimize this type of damage using pseudostatically determined design pressures.

A recent design procedure uses the free earth support method and Rowe's moment reduction method, with earthquake effects represented by pseudostatic inertial forces. A brief summary of the procedure is presented below; a detailed description with a worked example may be found in Ebeling and Morrison (1993).

1. Design the anchored bulkhead for static loading conditions.
2. Select pseudostatic accelerations a_h and a_v.
3. Compute the active soil thrust on the back of the wall using the M-O method. The active wedge is assumed to originate at the bottom of the wall.
4. Compute the passive soil thrust acting on the front of the wall using the M-O method. The passive wedge is also assumed to originate at the bottom of the wall.
5. Compute the minimum required depth of wall penetration by summing moments about the wall–tierod connection. All water pressures (hydrostatic, hydrodynamic, and excess porewater, if present) must be included.

6. Compute the required anchor resistance by summing the horizontal forces acting on the wall. All water pressures (hydrostatic, hydrodynamic, and excess porewater, if present) must be included. The computed anchor resistance is termed the *free earth support anchor resistance.*
7. Compute the distribution of bending moments over the height of the wall. All water pressures (hydrostatic, hydrodynamic, and excess porewater, if present) must be included. The maximum bending moment is termed the *free earth support moment.*
8. Compute the design bending moment as the product of the free earth support moment and Rowe's moment reduction factor (Rowe, 1952).
9. Set the design tierod force at a level 30% greater than the free earth support anchor resistance.
10. Determine the required size of the anchor block to satisfy horizontal force equilibrium considering the active and passive pressures, as well as all water pressures, on both sides of the block. The effects of any water pressures on the bottom and top surfaces of the anchor block should also be considered.
11. Locate the anchor block at a sufficient distance behind the wall that the active wedge behind the wall does not intersect the passive wedge in front of the anchor block. Since the active and passive failure surfaces are flatter for seismic loading than for static loading, seismic design may require a considerably longer tierod than static design.
12. Check the effects of redistribution of any earthquake-induced excess porewater pressure after earthquake shaking has ended.

Case histories of anchored bulkhead performance (neglecting cases in which widespread liquefaction was observed) suggest that anchored bulkhead damage levels can be predicted approximately with the aid of two dimensionless indices: the *effective anchor index* and the *embedment participation index* (Gazetas et al., 1990). Referring to Figure 11.21a, the effective anchor index describes the relative magnitude of the available anchor capacity as

$$\text{EAI} = \frac{d}{H} \tag{11.48}$$

where d is the horizontal distance between the active wedge and the tierod–anchor connection and H is the height of the wall. The critical active failure plane is taken to originate at the effective *point of rotation* of the wall, which can be located using soil–structure interaction analyses or estimated as

$$f \approx \left(\frac{1 + k'_e}{2} - \frac{\phi - 20^\circ}{50^\circ} \right) H \leq D \tag{11.49}$$

where

$$k'_e = \begin{cases} \dfrac{k_h}{1 - k_v} & \text{above the water table} \\ \dfrac{(a_h/g)_{\max}}{1 - 2(a_v/g)_{\max}/3} & \text{below the water table} \end{cases}$$

The inclination of the critical active failure plane can be approximated (Dennehy, 1985) as

$$\alpha_{AE} \approx 45° + \frac{\phi}{2} - 135°(k'_e)^{1.75} \tag{11.50}$$

for $0.10 \leq k'_e \leq 0.50$ and $25° \leq \phi \leq 35°$. Beyond these ranges, equation (11.17) can be used to estimate the inclination of the active wedge. The embedment participation index is defined as

$$\text{EPI} = \frac{F_{PE}}{F_{AE}}\left(1 + \frac{f}{f + H}\right) \tag{11.51}$$

where F_{AE} and F_{PE} are the potential active and passive thrusts, respectively. For uniform backfill and foundation soils,

$$\text{EPI} \approx \frac{K_{PE}}{K_{AE}} r^2(1 + r) \tag{11.52}$$

where $r = f/(f + H)$. Values of EAI and EPI have been computed for 75 anchored bulkheads for which degrees of damage in earthquake had been categorized as indicated in Table 11-5 (Gazetas et al., 1990). Comparison of degrees of damage with EAI and EPI showed significant trends in the characteristics of anchored bulkheads that performed well and those that performed poorly. As illustrated in Figure 11.21b, anchored bulkheads with high EAI and EPI values (zone I) generally suffered little or no damage. Anchored bulkheads with low EAI and EPI values (zone III) usually suffered severe damage. Moderate damage was generally associated with intermediate combinations of EAI and EPI (zone II). The chart of Figure 11.21b is a very useful tool for checking the design of anchored bulkheads in waterfront areas.

Table 11-5 Qualitative and Quantitative Descriptions of Reported Degrees of Damage to Anchored Bulkheads during Earthquakes

Degree of Damage	Description of Damage	Permanent Horizontal Displacement at Top of Sheetpile (cm)
0	No damage	< 2
1	Negligible damage to the wall itself; noticeable damage to related structures	2–10
2	Noticeable damage to the wall	10–30
3	General shape of anchored sheetpile preserved, but significantly damaged	30–60
4	Complete destruction	> 60

Source: After Kitajima and Uwabe (1979).

Tieback Walls. Because their use was originally restricted to temporary support of excavations, the seismic performance of tieback walls has received relatively little attention. As permanent tieback walls have become more common, however, recognition of the need to consider seismic loading in their design has increased. With respect to seismic performance, tieback walls are similar to anchored bulkheads—the primary differences are that tieback walls have multiple anchors and that the anchors are generally inclined. Although

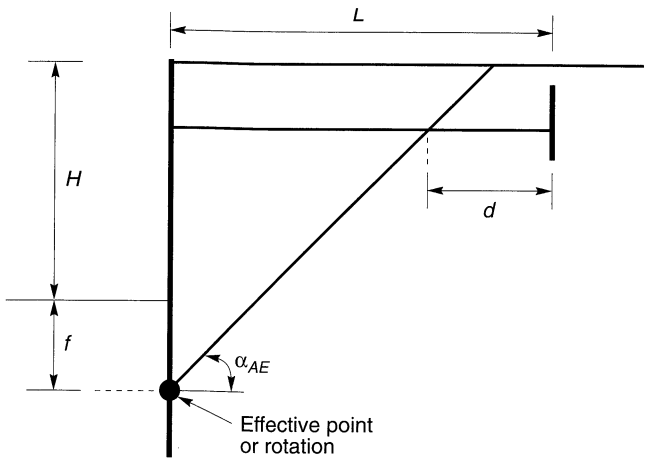

Figure 11.21 (a) Geometry and notation for evaluation of anchored bulkhead design; (b) correlation between damage levels and dimensionless anchored bulkhead indices. After Gazetas et al. (1990). Empirical design method for waterfront anchored sheetpile walls, *Design and Performance of Earth Retaining Structures.* Reprinted by permission of ASCE.

formalized design procedures are not currently available, the results of a limited number of experimental and numerical investigations provide insight into special considerations for seismic design of tieback walls. Few observations of the seismic performance of tieback walls have been made, but those that are available generally indicate good performance (Ho et al., 1990).

Numerical analyses indicate that the stiffness and spacing of the anchors strongly influences the permanent displacements of a tieback wall (Siller and Frawley, 1992). In general, tieback walls with stiff anchors will develop smaller permanent displacements than walls with softer anchors. Tieback walls with smaller vertical spacing between anchors will experience smaller and more uniform permanent displacements than walls with greater anchor spacing. Earthquake-induced permanent displacements also appear sensitive to static design pressures—walls designed for higher static pressures suffer smaller permanent displacements during earthquakes than walls designed for lower static pressures. Tieback walls also tend to develop smaller permanent when higher rather than lower initial anchor preloads are used (Siller and Dolly, 1992).

Tieback walls can also be influenced by phase differences between the response of the soil behind the wall and the foundation soil (Fragaszy et al., 1987). Wall elements that extend into the foundation soils may be subjected to very high bending moments at the base of the wall. Further, inclined anchors that extend below the bottom of the excavation may experience very high tensile forces when the soil end moves one way and the wall end the other.

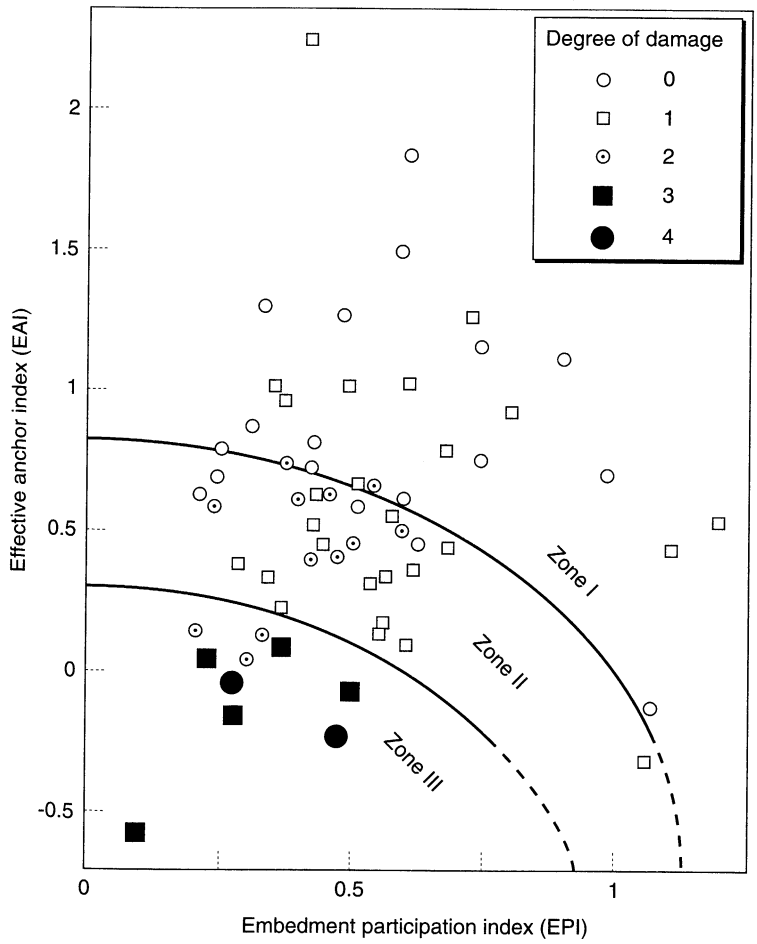

(b)

Figure 11.21 *(continued)*

11.8.4 Reinforced Soil Walls

Reinforced soil walls have become very popular in recent years. Although many different materials are used, reinforced soil walls consist of a zone of reinforced soil that retains unreinforced soil behind it. During an earthquake, a reinforced soil wall is subjected to a dynamic soil thrust at the back of the reinforced zone and to inertial forces within the reinforced zone in addition to static forces. The wall must be designed to avoid *external instability* (sliding or overturning failure of the reinforced zone) and *internal instability* (tensile or pullout failure of the reinforcement). Current design procedures, such as those described below (Christopher et al., 1990), use a pseudostatic approach, but displacement-based design procedures are likely to be developed in the future.

Reinforced soil walls use different materials and provide support by different mechanisms than do conventional retaining walls. Their design requires careful consideration of loading, time, and environmental factors that may not be significant for conventional retaining walls. The following sections are restricted to seismic aspects of reinforced soil wall design. Other aspects of design are discussed in detail by Mitchell and Villet (1987), Christopher et al. (1990), and Koerner (1994).

11.8.4.1 External Stability

For evaluation of external stability, a reinforced wall is treated much like a gravity wall. As illustrated in Figure 11.22, the reinforced zone is assumed to be acted on by its own weight, W, and the static soil thrust, P_A. Earthquake loading is represented pseudostatically by the dynamic soil thrust, ΔP_{AE}, and the inertial force on the reinforced zone, P_{IR}. The external stability of a particular wall design can be evaluated by the following procedure:

1. Determine the peak horizontal ground surface acceleration, $a_{\max}$.
2. Calculate the peak acceleration at the centroid of the reinforced zone from the equation

$$a_c = \left(1.45 - \frac{a_{\max}}{g}\right) a_{\max} \tag{11.53}$$

3. Calculate the dynamic soil thrust from

$$\Delta P_{AE} = 0.375 \frac{a_c \gamma^{(b)} H^2}{g} \tag{11.54}$$

where $\gamma^{(b)}$ is the unit weight of the backfill soil.

4. Calculate the inertial force acting on the reinforced zone from

$$P_{IR} = \frac{a_c \gamma^{(r)} HL}{g} \tag{11.55}$$

where $\gamma^{(r)}$ is the unit weight of the reinforced zone.

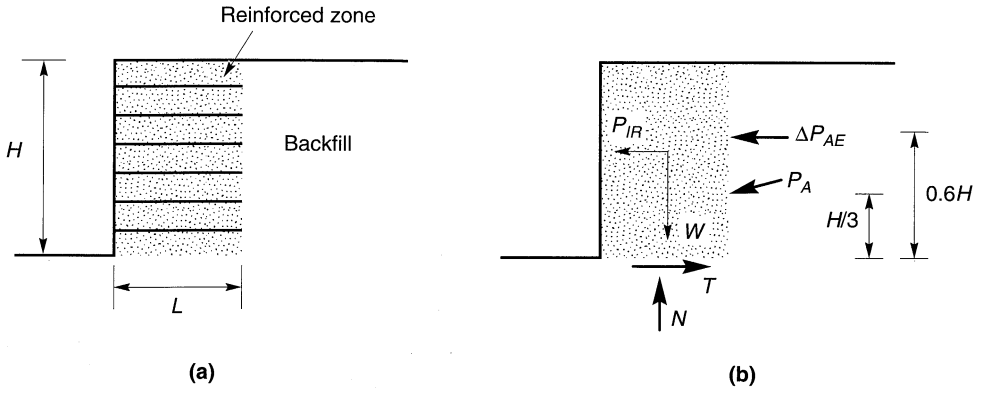

Figure 11.22 (a) Geometry and notation for reinforced soil walls; (b) static and pseudostatic forces acting on reinforced zone.

5. Add P_{AE} and 50% of P_{IR} to the static forces acting on the reinforced zone and check sliding and overturning stability (the reduced value of P_{IR} is allowed to account for the fact that the maximum values of ΔP_{AE} and P_{IR} are unlikely to occur at the same time). For seismic design, factors of safety against sliding and overturning should be greater than or equal to 75% of the minimum acceptable factors of safety for static loading.

11.8.4.2 Internal Stability

Internal stability evaluation depends on the nature of the reinforcement since the critical internal failure surface is different for inextensible and extensible reinforcement (Figure 11.23). Internal stability for seismic conditions can be evaluated in the following steps:

1. Determine the pseudostatic inertial force acting on the potentially unstable internal failure zone,

$$P_{IA} = \frac{a_c W_A}{g} \tag{11.56}$$

where W_A is the weight of the failure mass (the trapezoidal or triangular zones in Figure 11.23a and b for inextensible or extensible reinforcement, respectively).

2. Distribute P_{IA} to each reinforcement layer in proportion to its resistant area (the area of reinforcement that extends beyond the potential internal failure surface). This process produces a dynamic component of tensile force for each layer of reinforcement.
3. Add the dynamic components of tensile force to the static components of tensile force to obtain the total tensile force for each layer of reinforcement.
4. Check to see that the allowable tensile strength of the reinforcement is at least 75% of the total tensile force in each layer of reinforcement.
5. Check to see that each layer of reinforcement extends far enough beyond the potential internal failure surface to avoid pullout failure with a factor of safety not less than 75% of the minimum static factor of safety when the total tensile force is applied.

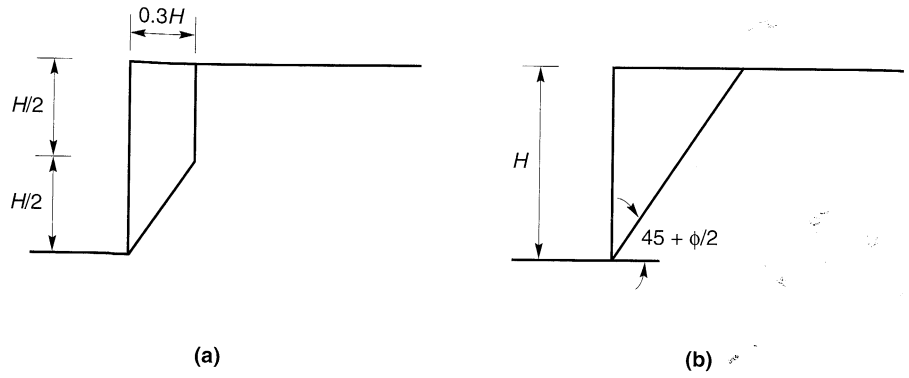

Figure 11.23 Critical potential failure surfaces for evaluation of internal seismic stability of reinforced soil walls: (a) inextensible reinforcement; (b) extensible reinforcement.

11.9 SUMMARY

1. A variety of different systems are used to retain soil; many innovative systems have been developed and used in the last 20 years. For seismic design purposes, most retaining systems fall into three general categories: gravity walls, cantilever walls, and braced walls. Each of these types of walls resists the lateral pressures of the retained soil differently.
2. Retaining walls can fail in many different ways. Gravity walls fail by sliding, overturning, or gross instability. Cantilever walls can fail in the same ways as gravity walls, but can also fail in bending. Braced walls can fail in the same ways as cantilever walls, but also by bracing element failure or rotation about the brace connection.
3. The seismic performance of a retaining wall depends on the total pressures (i.e., static plus dynamic pressures) that act on it during an earthquake. Consequently, the level of dynamic pressures required to damage the wall depends on the level of static pressures that exist before the earthquake. Analysis of the seismic behavior of a retaining wall, therefore, requires an initial analysis of the behavior under static conditions.
4. The seismic response of retaining walls is a complex example of soil–structure interaction. Because of this complexity, design procedures are usually based on a number of simplifying assumptions. Although the simplified procedures do not represent all aspects of wall–soil behavior accurately, they have been shown to provide a reasonable basis for design.
5. The soil pressure on a retaining wall depends on whether the wall is able to move relative to the soil. The dynamic pressures acting on a yielding wall are usually estimated by the pseudostatic Mononobe–Okabe analysis. The dynamic pressures on nonyielding walls are usually estimated by an elastic analysis.
6. The presence of water on either side of a retaining wall strongly influences the seismic behavior of the wall. Water on the outboard side of the wall can exert dynamic, in addition to hydrostatic, pressures on the face of the wall. Water within the backfill can influence the inertial forces acting on the wall and can develop hydrodynamic or excess porewater pressures.
7. Earthquake-induced displacements of retaining walls can be estimated by procedures analogous to the Newmark sliding block analysis for displacements of slopes. Refinements to this approach allow consideration of factors such as backfill amplification, wall tilting, kinematic constraints, and vertical acceleration. Procedures for estimation of probabilities of various displacement levels are also available.
8. Seismic design of retaining walls is generally based on seismic pressures or allowable displacements. In the former approach, pseudostatic or pseudodynamic analyses are used to estimate seismically induced wall pressures, and the wall is designed to resist those pressures without failing or causing failure of the surrounding soil. The latter approach involves designing the wall such that its seismically induced permanent displacement does not exceed a predetermined allowable displacement.
9. The majority of observed failures of retaining walls during earthquakes have occurred in waterfront areas; many have involved liquefaction of the backfill. Excessive permanent displacements of anchored bulkheads in waterfront areas have often been associated with inadequate wall embedment depths and/or insufficient anchor capacity.

HOMEWORK PROBLEMS

11.1 Compute the static thrust and overturning moment at the base of the concrete retaining wall shown below.

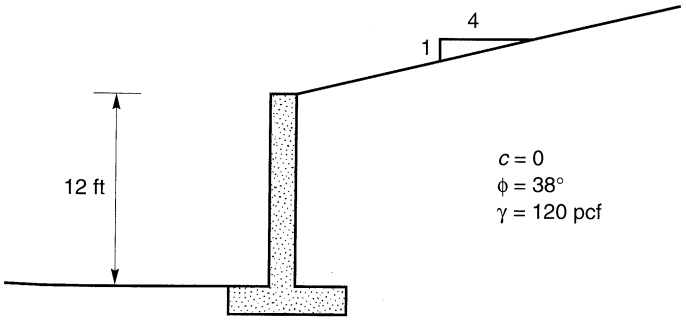

Figure P11.1

11.2 The wall shown in Problem 11.1 is subjected to earthquake shaking with a peak horizontal acceleration of $0.28g$. Assuming a pseudostatic coefficient, $k_h = 0.3\ a_{max}/g$, estimate (a) the total active thrust acting on the wall, (b) the height of the resultant of the total active thrust, and (c) the total overturning moment about the base of the wall.

11.3 Using the Steedman–Zeng approach, plot the distributions of maximum and minimum lateral pressure if the wall shown below is subjected to a $0.15g$ harmonic base motion at (a) a frequency of 0.5 Hz, and (b) a frequency of 5.0 Hz.

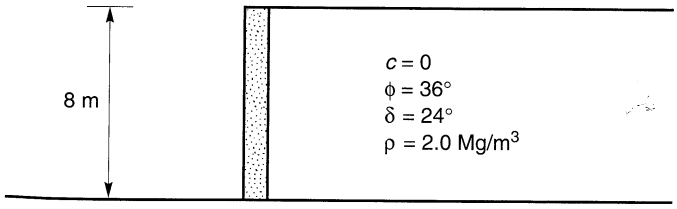

Figure P11.3

11.4 A 12 ft deep rigid basement wall is backfilled with dense gravelly sand: $c = 0$, $\phi = 45°$, $\gamma = 140$ pcv. Estimate the maximum dynamic thrust acting on the wall when subjected to a ground motion with $a_{max} = 0.33g$.

11.5 Compute the yield acceleration for the concrete gravity wall shown below.

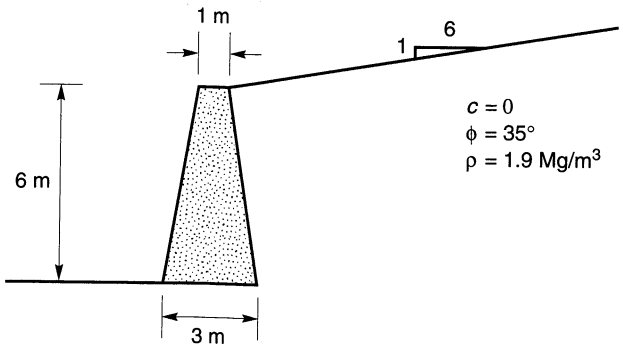

Figure P11.5

11.6 Using the Richards–Elms procedure, estimate the permanent displacement of the wall of Problem 11.5 when subjected to (a) the Gilroy No. 1 (rock) ground motion, and (b) the Gilroy No. 2 (soil) ground motion.

11.7 Using the Whitman–Liao procedure, estimate the permanent displacement of the wall of Problem 11.5 when subjected to (a) the Gilroy No. 1 (rock) ground motion, and (b) the Gilroy No. 2 (soil) ground motion.

11.8 Estimate the permanent displacement of the wall in Problem 11.5 that would have a 10% probability of exceedance if subjected to the Gilroy No. 2 (soil) motion.

11.9 A 15 ft tall gravity wall is to retain a level sand backfill ($c = 0$, $\phi = 35°$, $\gamma = 115$ pcf). The wall will be placed on a layer of dense sandy gravel ($c = 0$, $\phi = 44°$, $\gamma = 140$ pcf). Determine the wall weight that would be required to limit the permanent displacement of the wall to 1/4-inch if subjected to the Gilroy No. 2 (soil) ground motion.

11.10 The anchored bulkhead shown below is located in a seismically active area. Neglecting the effect of vertical motions, estimate the minimum peak acceleration levels that would be likely to produce (a) moderate damage, and (b) severe damage.

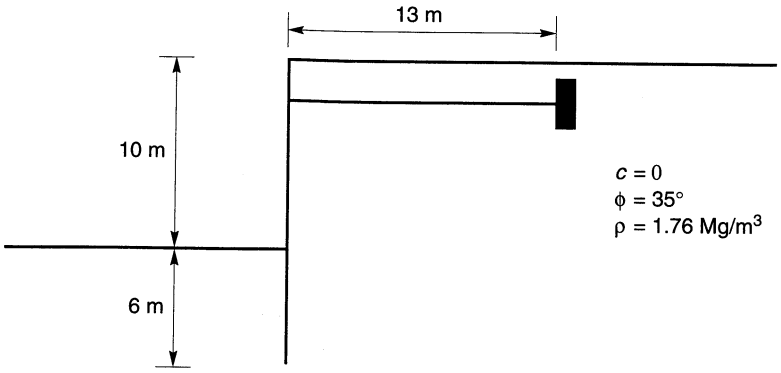

Figure P11.10